Pedogenic carbonate as a transient soil component in a humid, temperate forest (Michigan, USA)

Submitted to Quaternary Research

Julia R. Kelson[a,b*], Tyler E. Huth[a,c], Kirsten Andrews[a], Miriam N. Bartleson[a], Thure E. Cerling[d], Lixin Jin[e], Matthew P. Salinas[a], Naomi E. Levin[a]

[a] Department of Earth and Environmental Sciences, University of Michigan, Ann Arbor MI 48109

[b] Department of Earth and Atmospheric Sciences, Indiana University, Bloomington IN 47405

[c] Department of Earth, Environmental, and Planetary Sciences, Washington University in St. Louis, St. Louis MO 63130

[d] Geology and Geophysics, University of Utah, Salt Lake City, UT 84112

[e] Department of Geological Sciences, University of Texas at El Paso, TX 79968

*Corresponding author. Email: jrkelson@iu.edu, Phone: (812) 855-5582

ABSTRACT

In humid, continental Michigan, we identified pedogenic carbonate in a soil profile developed on glacial drift sediments, as rinds, rhizoliths and filaments (at depths > 50 cm). Given that the climate setting is unusual for pedogenic carbonate, we investigated its formation with environmental monitoring and isotope analyses of carbonate ($\delta^{13}C$, $\delta^{18}O$, Δ_{47} and ^{14}C) and waters ($\delta^{18}O$ and $\delta^{2}H$). We found covariation in $\delta^{13}C$ and Δ_{47} amongst the carbonate types (rhizoliths, rinds, filaments, bulk soil, and detrital clasts), and ^{14}C ages of rinds that pre-date plausible formation ages. The $\delta^{13}C$ and Δ_{47} values of the bulk carbonate and some of the pedogenic morphologies are not fully compatible with pedogenic formation in the modern environment. The $\delta^{18}O$ data from precipitation and river waters and from carbonates are not uniquely identifying; they are compatible with the soil carbonate being pedogenic, detrital, or a mix. We conclude that the soil carbonate is likely a physical mix of pedogenic and detrital carbonate. Pedogenic carbonate is forming in this humid setting, likely because seasonal cycles in soil respiration and temperature cause cycles of dissolution and re-precipitation of detrital and pedogenic carbonate. The pedogenic carbonate may be transient feature as carbonate-rich till undergoes post-glacial chemical weathering.

Key words: inorganic soil carbon, pedogenic carbonate, clumped isotopes, chemical weathering, temperate forests

INTRODUCTION

Soil carbonate is a significant component of the global carbon cycle, comprising 40-50% of total global soil carbon (Eswaran et al., 2000; Plaza et al., 2018). The term ‘soil inorganic carbon' or 'soil carbonate' is used to describe carbonate in soil that is pedogenic, detrital, or biogenic in origin (Monger et al., 2015; Zamanian et al., 2016). 'Pedogenic' carbonate refers to carbonate that precipitates *in situ* in soil pore water. 'Detrital' carbonate refers to carbonate inherited from parent carbonate material, such as finely ground limestone or dust. Biogenic carbonate forms as animal or plant skeletons (e.g., shells or seeds). Amongst these three forms of soil carbonate, pedogenic carbonate is of particular interest because it represents active fluctuations in the pools of soil inorganic carbon. Furthermore, pedogenic carbonate is commonly used as a paleoclimate archive because its stable isotope composition is related to environmental conditions at the time of its formation (e.g., Cerling and Quade, 1993; Kelson et al., 2020).

Pedogenic carbonate is most commonly found and studied in drylands, where the balance between limited rainfall and high evaporation is thought to promote the accumulation of calcites (e.g., Arkley, 1963; Royer, 1999; Retallack, 2005; Breecker et al., 2009; Slessarev et al., 2016).Though less explored, humid environments host as much as 20% of the global stock of soil carbonate (Plaza et al., 2018; United States Department of Agriculture, Natural Resources Conservation Service, 2022), some of which is interpreted to have a pedogenic origin (Cerling, 1984; Strong et al., 1992; Wang et al., 1993; Railsback, 2021; Licht et al., 2022). An understanding of the origin and the processes driving the formation of pedogenic carbonate in humid environments would therefore help understand the factors that contribute to spatial variation in soil carbonate (Slessarev et al., 2016; Stanbery et al., 2017; Pfeiffer et al., 2023). Understanding the distribution of pedogenic carbonate is important to help inform predictions of how its global distribution might evolve under climate change and anthropogenic management

(Nyachoti et al., 2019; Ferdush and Paul, 2021; Naorem et al., 2022; Wani et al., 2023; Stanbery et al., 2023). Furthermore, pedogenic carbonate can be either a net sink or source of carbon to the atmosphere (e.g., Monger et al., 2015; Sharififar et al., 2023). If pedogenic carbonate is precipitating as an intermediate step during lithogenic carbonate weathering, it may slow the export of dissolved bicarbonate and alter carbon cycling rates (Szramek and Walter, 2004; Williams et al., 2007).

Here we document an occurrence of pedogenic carbonate in glacial drift in the humid continental climate of southern Michigan. Building on prior local work on carbonate weathering in the shallow vadose zone (Jin et al., 2008b, a, 2009), we use environmental monitoring and isotope geochemistry to explore the origin and formation conditions of the soil carbonate at a site in southern Michigan. We infer the processes driving pedogenic carbonate formation at our site, and discuss its implications for paleoclimate reconstructions, regional chemical weathering, and carbon cycling.

METHODS

We investigated soil carbonate formation in southern Michigan (USA) using soil stratigraphy, soil monitoring, water isotope analyses, and carbonate isotope analyses. We first describe the site and modern climate. Then we describe sampling, monitoring, and isotope analysis methods.

Site description

The study site is in the Edwin S. George Reserve (hereafter, “the Reserve”), which is a forest preserve maintained by the University of Michigan (UM), located in southern Michigan, USA (Figure 1) (42°27.44'N 83°59.87'W WGS84). Southern Michigan has a humid continental climate. Regional precipitation averages 860 mm/year, well above the ~500 mm/year threshold commonly used to delineate where soils contain abundant calcium carbonate (i.e., the Pedocal/Pedalfer boundary) (D’Avello et al., 2019). Each month has >50 mm precipitation, with May through August being the wettest four months and precipitation primarily falling as snow from November through April. The mean annual air temperature is 8.8 °C (winter mean = -3.4 °C, summer mean = 20.8 °C) (Arguez et al., 2012).

The geomorphology and topography of the region was strongly influenced by the growth and retreat of the Laurentide Ice Sheet (Dalton et al., 2020), as reflected in sand- and gravel-rich soils, numerous kettle lakes and swamps, and eskers (Rieck, 1976; Farrand and Bell, 1982; Schaetzl, 2001). Glacial sediments are derived from Canadian shield bedrock and from the sedimentary sequence of Paleozoic and Mesozoic rocks in the Michigan Basin, which include limestones and dolomites (Milstein, 1987; Williams et al., 2007). The glacially reworked sediments in Michigan contain finely-ground dolomites and limestones (Schaetzl, 1992; Williams et al., 2007; Jin et al., 2008b), resulting in soil series with mappable amounts of soil carbonate that are a global outlier for their high pH despite the humid climates (Slessarev et al., 2016; United States Department of Agriculture, Natural Resources Conservation Service, 2022). The study site is a knoll about 10 m high that was partially excavated during a gravel quarry operation initiated between 1950 and 1966 (Figure 2, Figure 3). Most of the Reserve is forested, including the top of the knoll. The near-vertical, excavated slope itself is unvegetated. The native vegetation of the study site is a mixed oak forest with oak, tamarack, and willow (Roller, 1974; Comer et al., 1995). The forest is dominated by C_3 vegetation: $\delta^{13}C$ values of soil organic matter from the Reserve range from -29.4 to -24.7‰, with an average of -26.8 ‰ (Jin et al., 2009).

Soil stratigraphy and sample collection

We characterized the Reserve site with soil stratigraphic techniques and monitoring of modern below-ground conditions. We described the stratigraphy in a hand-dug soil pit and in the existing cut slope after we cleared it vegetation and then further machine-excavated. Field descriptions included depth and thickness of soil and sedimentary horizons, the morphology of clay films and soil carbonate, grain size, and structure (Birkeland, 1984) (Figure 3).

We collected soil, sediment, and water samples. The soil and sediment samples included several morphologies of soil carbonate, including rhizoliths, rinds on the bottoms of clasts (< 1 mm thick), thin filaments ("stringers"), diffuse carbonate in the soil matrix, bulk sediment (matrix), and limestone/dolostone clasts. We collected water samples from within and outside of the Reserve. Within the Reserve, the soil water and surface water from East Marsh were opportunistically collected (fall 2020 to fall 2022) (n = 12 marsh samples, n = 29 soil water samples collected on 12 unique events). We collected bulk soil for soil water sampling when soil pits were dug for monitoring installation and then subsequently with a hand auger (typical depths of 10, 25, and 50 cm). We extracted the soil water from the bulk soil samples via a custom-built, cryogenic vacuum extraction line at UM (largely following that of West et al., 2006). Outside of the Reserve, we implemented a longer-term precipitation and river monitoring program in nearby Ann Arbor, Michigan (30 km distant, Figure 1) (started fall 2018, ongoing). Weekly precipitation samples were collected with a no-oil collector (after Gröning et al., 2012). Weekly Huron River samples were initially collected from a dock upstream of the Argo Dam (May-October 2018) and subsequently downstream from the Fuller Street bridge (October 2018 to present, with a hiatus in summer 2020). We collected water and bulk soil samples into vials with polycone seal caps; caps were then wrapped with Parafilm as a secondary barrier to evaporation. We stored the vials upside down at room temperature at UM until analysis.

To further characterize the modern soil system, we monitored soil temperature and soil moisture at depths of 10, 30, and 60 cm and soil CO_2 concentration (pCO_2) at 60 cm (Figure 4). We monitored soil temperature with a HOBO Pendant, soil moisture with a HOBO RX3000 Remote Monitoring Station equipped with HOBOnet Soil Moisture EC-5 Sensors, and soil CO_2 concentration with a CO2meter.com K33 ELG sensors capable of analyzing 0–10,000 ppm CO_2. The monitoring regime covered winter 2021 to winter 2022, with gaps due to equipment failure.

Isotope analytical methods

We analyzed water and carbonate isotope compositions to investigate the conditions of soil carbonate formation.

Water stable isotope analyses

We measured the oxygen and hydrogen ($\delta^{18}O$ and $\delta^{2}H$) compositions of meteoric and water samples (Figure 5). All water samples were introduced to instrumentation as liquid water. The $\delta^{18}O$ and $\delta^{2}H$ were measured via Cavity Ring Down Spectrometry primarily at UM and secondarily at Washington University in St Louis (WU). The UM system consists of a Picarro A0325 Autosampler, A0211 Vaporizer, and A0214 Micro-Combustion Module connected to a Picarro L2130-i Analyzer. We normalized the isotope values to the VSMOW scale using four in-house liquid water standards that are referenced to USGS water standards (USGS45, 46, 49, and 50). Precision is typically better than 0.1 ‰ in $\delta^{18}O$ and 0.5 ‰ in $\delta^{2}H$ based on repeat measurements of deionized water (Aron et al., 2020). The WU system consists of a Picarro

A0325 Autosampler, A02 Vaporizer, and A0214 Micro-Combustion Module connected to a Picarro L2140-i Analyzer that was run with two lasers activated (i.e., the ^{17}O-mode). We normalized the samples to VSMOW2 and SLAP2 using in-house liquid waters and international reference waters (Hutchings and Konecky, 2023). Typical RMSE of known waters is 0.1 ‰ in $\delta^{18}O$ and 0.5 ‰ in $\delta^{2}H$. For water samples with replicate measurements, typical standard deviations are 0.1 ‰ in $\delta^{18}O$ and 0.2 ‰ in $\delta^{2}H$. We report *d*-excess as secondary isotope parameter for all water samples (*d*-excess = $\delta^{2}H - 8\times\delta^{18}O$).

Carbonate carbon, oxygen, and clumped stable isotope analytical methods

We processed several distinct carbonate morphologies for isotope analysis. We hand-picked gravels from the bulk sediment. For rinds and rhizoliths, we brushed the soil off the outer surface. We then carefully removed the rind material from the parent clast with a hand drill. We homogenized and crushed the cleaned rhizoliths. We hand-picked thin filaments of carbonate ("stringers") out of the soil matrix and then homogenized the material. We cut open limestone/dolostone clasts and then subsampled the cut surface with a hand drill.

We measured carbonate $\delta^{13}C$ and $\delta^{18}O$ (hereafter $\delta^{13}C_c$ and $\delta^{18}O_{c)}$ using a Kiel IV automated preparation device connected online to an isotope ratio mass spectrometer (a Delta V or a ThermoFisher MAT 253) at UM, standardized with NBS-19 to the VPDB scale. Typical standard deviations of known values are < 0.1 ‰ for $\delta^{13}C$ and $\delta^{18}O$.

Clumped isotope (Δ_{47}) geochemistry refers to the temperature-dependent clumping between ^{13}C and ^{18}O in a carbonate mineral (Eiler, 2007; Huntington and Petersen, 2023). For Δ_{47} analyses, we prepared samples on a custom, automated vacuum extraction line connected to a Nu Perspective at the Isotopologue Paleosciences Laboratory at UM. First, 6-9 mg of carbonate equivalent of sample material was acidified in a common bath of phosphoric acid held at 90 °C. The resulting CO_2 was passed with helium through cryogenic water traps and a

Poropak Q column. We calculated the Δ_{47} values using the ^{17}O parameters of Brand et al. (2010) (Schauer et al., 2016; Daëron et al., 2016) and projected them into the ICDES90 reference frame (Bernasconi et al., 2021; Daëron, 2021) using online equilibrated and heated gases (30 °C and 1000 °C) and carbonate standards ETH1-3. Typically, the standard deviation of Δ_{47} values of each standard is < 0.02 ‰ within a session, and the long-term standard deviation of an in-house standard (102GCAZ01) is 0.014 ‰. We calculated temperatures (hereafter $T\Delta_{47}$) using the empirical calibration of Anderson et al. (2021) ($\Delta_{47} = 0.0391 * 10^6/T^2 + 0.154$).

Strontium isotope analyses

We selected two carbonate rind samples for strontium isotope analysis ($^{87}Sr/^{86}Sr$), which was carried out at the University of Utah's ICP-MS Metals and Strontium Isotope Facility. About 50 mg of ground carbonate was digested in 0.5 mL of concentrated HNO_3 at room temperature and then diluted with Type I grade water. Strontium concentration in acid digest was determined using an external calibration curve prepared from a single element Sr standard (Inorganic Ventures, Christiansburg, VA, US) in a triple quadrupole inductively coupled plasma mass spectrometer (ICPMS, Agilent 8900, Santa Clara, CA, US). Aliquots from the digests containing 200 ng of Sr were then mixed with concentrated HNO_3 and water to 2 M HNO_3 and purified using an automated system (PrepFAST MC, Elemental Scientific, Omaha, NE, US). $^{87}Sr/^{86}Sr$ ratios were corrected for mass bias using an exponential law and normalizing to $^{86}Sr/^{88}Sr = 0.1194$ (Steiger and Jäger, 1977). To correct for isobaric interferences (e.g., from ^{87}Rb and ^{86}Kr), ^{85}Rb and ^{83}Kr were simultaneously monitored using the corresponding invariant ratios of $^{87}Rb/^{85}Rb = 0.385706$ and $^{86}Kr/^{83}Kr = 1.502522$ (Steiger and Jäger, 1977). Measurement accuracy was assessed via multiple analyses of standard reference material SRM 987 in each run, with an analyzed value of 0.710297 ± 0.000006 (n = 8; mean ± standard deviation)

compared to the certified value of 0.71034 ± 0.00026. Analytical precision (standard error) of $^{87}Sr/^{86}Sr$ for all samples was <0.00001.

Radiocarbon dating

We selected two carbonate rinds from the soil pit (50 and 70–75 cm depth) for radiocarbon analysis. 10 mg of chipped samples were sent to the University of Arizona's AMS Laboratory where CO_2 was extracted and purified, graphitized, and analyzed. We calculated the calibrated radiocarbon ages (cal yr BP) using the CALIB 8.0 software with the IntCal09 calibration curve (Stuiver and Reimer, 1993; Reimer et al., 2009) (Table 1) (Supplementary Table S1).

Conceptual models for soil carbonate genesis and predictions for its stable isotope composition

We used previously established relationships between the stable isotopic composition of pedogenic carbonate ($\delta^{13}C$, $\delta^{18}O$, and Δ_{47}) and its formation environment to predict the stable isotope composition of soil carbonate under three scenarios that involve formation in equilibrium with climate conditions at the Reserve (open and closed system) and its mixing with detrital carbonate (Figure 6). We employed a simple mixing model to explore the possibility is that the soil carbonate is pedogenic carbonate mixed with detrital carbonate particles (Amundson et al., 1988; West et al., 1988b; Kraimer and Monger, 2009; Zhou and Chafetz, 2010; Michel et al., 2013) (Figure 6a). We modeled linear mixing in $\delta^{18}O$-$\delta^{13}C$ and $\delta^{13}C$-Δ_{47} between various potential endmembers and with varying fraction of pedogenic carbonates (F) in a Monte Carlo framework (Figure 7). An example mixing line is shown in Figure 6 (schematically in a and b, calculated in g and h). In the Monte Carlo mixing framework (Figure 7), we allow for a range of

endmember compositions (Supplementary Code). We allowed a range in detrital endmember compositions that was informed by the measured isotopic composition of limestone clasts at the site and the secular isotopic trends through the Phanerozoic (Veizer et al., 1999): $-8 \leq \delta^{18}O \leq -5$, $-2 \leq \delta^{13}C \leq +3$ ‰, and $0.448 \leq \Delta_{47} \leq 0.495$ ‰ ($65 \leq T\Delta_{47} \leq 91$ °C). For the pedogenic carbonate endmember, we allowed for a wide potential range of compositions that could be reasonably found for the vast majority of pedogenic carbonates found globally: $-15 \leq \delta^{18}O \leq -5$ ‰, $-14 \leq \delta^{13}C \leq 0$ ‰, $0.594 \leq \Delta_{47} \leq 0.678$ ‰ ($0 \leq T\Delta_{47} \leq 25$ °C) (e.g., Cerling, 1984; Kelson et al., 2020). Δ_{47} does not mix linearly, but the effect of nonlinearity in our range of values is ~0.0002 ‰ in Δ_{47} (White and Defliese, 2023), which is much smaller than our external precision in Δ_{47} (the long-term S.D. of our in-house standard, 102GCAZ01, is 0.014 ‰). Note, however, that there is nonlinearity between temperature and Δ_{47}; we perform the mixing calculations in Δ_{47} and then calculate temperature. We only used samples with $\delta^{13}C$, $\delta^{18}O$, and Δ_{47} data, and the feasible endmembers for each sample were those capable of reproducing the observed isotope composition within analytical error for all three isotopes (i.e., ±0.1 ‰ for $\delta^{13}C$ / $\delta^{18}O$, ± 5 °C for $T\Delta_{47}$). For visual clarity we calculated F values in increments of 0.1 and emphasize differences between increments by plotting their average values.

In a canonical calcic soil system, the soil pore water and CO_2 are open to isotopic exchange with incoming meteoric waters and the soil gas reservoir, resulting in a relatively small range in pedogenic carbonate isotope values that reflect formation in equilibrium with soil climate conditions (Figure 6b) (Cerling, 1984; Cerling and Quade, 1993; Quade et al., 2013). To model the pedogenic carbonate system, we first calculated the $\delta^{18}O$ values of the carbonate-parent water (i.e., reconstructed soil water, $\delta^{18}O_{rsw}$) using the temperature-dependent isotope fractionation factor informed by $T\Delta_{47}$ data (Kim and O'Neil, 1997) (Figure 5c). For samples without $T\Delta_{47}$ data, we use the average $T\Delta_{47}$ value to calculate $\delta^{18}O_{rsw}$. Choice of calibration for the fractionation factor does not materially change our interpretations (i.e., Coplen, 2007 vs. Kim

and O'Neil 1997). We compared the $\delta^{18}O_{rsw}$ to measured $\delta^{18}O$ values of meteoric and soil waters.

Then, we modeled the set of environmental conditions potentially capable of producing the measured soil carbonate $\delta^{13}C$ values using established equations that relate pedogenic carbonate to soil respiration, the overlying vegetation, and the atmosphere. For each sample, we first calculated the $\delta^{13}C$ of soil gas ($\delta^{13}C_s$) from the measured $\delta^{13}C$ of soil carbonate ($\delta^{13}C_c$) and its formation temperature (Romanek et al., 1992):

$$\varepsilon_{cl\text{-}CO2} = 11.98 - 0.12*T \quad (1)$$

where epsilon $\varepsilon_{cl\text{-}CO2}$ is the mineral-gas fractionation factor for calcite (i.e., $\delta^{13}C_s = (\delta^{13}C_c+1000)/(\varepsilon_{cl\text{-}CO2}/1000+1)-1000$).Then we modeled the $\delta^{13}C$ of soil respiration ($\delta^{13}C_r$) (Cerling, 1984; Cerling and Quade, 1993; Davidson, 1995):

$$\delta^{13}C_r = (\delta^{13}C_s -4.4 - C_a/C_s* \delta^{13}C_a + 4.4*C_a/C_s)/(1.0044-C_a/C_s*1.0044) \quad (2)$$

where C_a is atmospheric pCO_2 and C_s is soil pCO_2.This equation is solved independently for each measured $\delta^{13}C_c$ value, each representing a specific depth. The calculations were performed 10,000 times, assuming varying conditions within a plausible range for the late Quaternary (atmospheric CO_2 concentration: 180 to 280 ppm, soil CO_2 concentration: atmospheric concentration to 10,000 ppm; soil temperature: 0 to 25 °C; $\delta^{13}C$ of atmospheric CO_2: -6 to -7 ‰) (Cerling, 1984; Davidson, 1995; Bereiter et al., 2015; Eggleston et al., 2016; Huth et al., 2020) (Supplementary Code). The modeled conditions that were required to produce the measured $\delta^{13}C_c$ values were then compared to modern conditions (Figure 8).

RESULTS

Soil profile developed in carbonate-rich glacial drift

We documented a soil profile developed in stratified glacial drift. The soil profile is about 2.4 m thick and consists of two A horizons, a Bt horizon, and a Bk horizon (Figure 2; Figure 3). The parent material is fine-medium, poorly sorted sand with 10 - 15 % gravel; evidence of primary sedimentary bedding was not identified. Soil horizons (A1, A2, Bt, Bk, and Ck) were differentiated based on organic content, color, pedogenic structure, and secondary mineral composition (Figure 3). Notably, the Bk horizon was identified based on the presence of carbonate (i.e., the first depth at which the matrix reacted vigorously with hydrochloric acid application) and the sharp color change relative to the overlying layer. Within the Bk horizon, carbonate was found as Stage I-II rinds on the bottom of clasts, rhizoliths (some surrounding still-intact roots), stringers, and as diffuse fine-grained material within the matrix (Figure 2). The depth to the Bk horizon varied by up to 50 cm at several sampled locations (instrumented soil pit, auger collections, and the excavated slope) and at other test pits in glacial drift in the region; this variation could be partially due to alteration of the ground surface elevation during historical quarry operations and/or natural variation in leaching depths.

Below the soil profile, we found stratified sands and gravels consistent with a fluvio-glacial drift deposit, such as a kame or an esker (Figure 3). A layer of cross-bedded sand appears at 2.4 m below the surface. The sand unit is very fine to very coarse and well-rounded, with some grain size separation in the beds. There were abundant carbonate rhizoliths throughout the sand unit, and the matrix reacted vigorously with hydrochloric acid. The gravel unit 3.2 m below the ground surface consisted of lenses of sorted sediments, ranging from rounded -subrounded gravels to medium sand. The gravel unit reacted with HCl vigorously throughout, and many of the clasts displayed incipient (stage I) carbonate rinds (Figure 2; Figure 3).

Calcite mineralogy was confirmed with X-ray diffraction (XRD) analysis of rind material drilled from clasts collected at depths of 50 and 70 cm in a soil pit adjacent to the slope. The $^{87}Sr/^{86}Sr$ values of ≈0.709 for the rinds collected at 50 cm and 70-75 cm are consistent with marine limestone as the parent material (Table 1). The radiocarbon ages are 23,691 cal yr BP and 17,366 cal yr BP for the same rinds collected at 50 cm and 70-75 cm (Table 1).

Results of below-ground soil monitoring

Over the year of monitoring we conducted, we observed seasonal cycles in soil temperature, water content, and pCO_2. At carbonate-relevant depths of 60 cm, winter temperatures are near-freezing in January and February (0.6 °C). The soil begins to thaw mid-March, and temperatures reach a maximum temperature of 21.4 °C in late August (Figure 4). Soil water content remains at 0.2-0.3 m^3/m^3 for winter and spring (December through June), with minor fluctuations due to infiltration of snowmelt and precipitation. Initial snowmelt occurred in late February, causing an increase in water content at all depths that was followed by several cycles of increasing and decreasing soil moisture heading into the summer (Figure 4). The soil pCO_2 values were between 4300-4500 ppm midwinter (January to February). In late March, pCO_2 concentrations started to rise above winter lows, and then remained > 5000 ppm with spikes > 8000 ppm through early summer. Mid-late summer pCO_2 values (July to August) exceeded 10,000 ppm (the limit of our sensor). The pCO_2 record ended on August 11, 2021. Even considering the relatively short period of monitoring, these data capture the major seasonal trends (Figure 4).

Results of stable isotope analyses of carbonates and water and of predictions for pedogenic carbonate

The $\delta^{13}C_c$ values of all carbonates are -7.9 to 2.5 ‰ (VPDB), spanning a 10.4 ‰ range (Table 2; Figure 3; Figure 8). The $\delta^{13}C_c$ values of the rhizolith, stringer, and rind samples are generally lower than those of the bulk matrix and parent limestone clasts (Figure 3; Figure 6). The $\delta^{18}O_c$ values of all carbonates are -8.3 to -5.4 ‰ (VPDB), spanning a 2.9 ‰ range (Table 2; Figure 3; Figure 6; Figure 8). There is not marked differences in $\delta^{18}O_c$ values amongst carbonate morphologies (Figure 6). A subset of the samples was measured for Δ_{47}, and those values range from 0.4562 to 0.6219 ‰ (ICDES-90), corresponding to temperatures ($T\Delta_{47}$) of 87 to 16 °C (Table 3). The $T\Delta_{47}$ values of the measured rinds and rhizoliths are lower than the $T\Delta_{47}$ values of the limestone clasts (range of 15.9-32.9 °C vs. 70.2-86.6°C) (Table 3). There is significant covariation between $\delta^{13}C_c$ and $T\Delta_{47}$ (r^2 = 0.89, p = 0.004) amongst all the carbonate morphologies, but there is not covariation between $\delta^{18}O_c$ and $\delta^{13}C_c$ or $T\Delta_{47}$ (Figure 6d).

We observed seasonal variation in the isotopic values ($\delta^{18}O$, $\delta^{2}H$, and *d*-excess) of meteoric waters (Figure 5), typical of continental locations with seasonal fluctuations in air temperature (Clark and Fritz, 1991; Rozanski 1993). There is covariation between $\delta^{18}O$ and *d*-excess for samples with $\delta^{18}O$ > ~-10 ‰, indicative of evaporation. The local meteoric water line (i.e., $\delta^{18}O$-$\delta^{2}H$ linear regression) defined by precipitation has a slope of 7.8 that is close to the canonical value of 8 (Table 4) (Putman et al., 2019). The isotopic composition of the precipitation is quite variable ($\delta^{18}O$ ranges from -23.6 to -0.14 ‰ VSMOW, *d*-excess ranges from -8.5 to 25.8 ‰), though the isotopically light precipitation events tend to occur only in the winter and the isotopically heaviest rain occurs in the summer. The Huron River water has less variability in $\delta^{18}O$ and $\delta^{2}H$ than precipitation, but does have a sinusoidal pattern of seasonal variation (Figure 5), with low $\delta^{18}O$ values (high *d*-excess values) in the winter (typical minimum $\delta^{18}O$ of -9 ‰ and maximum *d*-excess of +15) and high $\delta^{18}O$ values (low *d*-excess values) in the

summer (typical maximum $\delta^{18}O$ of -5 and minimum *d*-excess of +5) (Pelletier, 2020). East Marsh in the Reserve has $\delta^{18}O$ values that are consistently higher than the contemporaneous river water and the $\delta^{18}O$-$\delta^{2}H$ relationship has a slope of 5.4, indicating evaporative influences (Table 4). The soil water isotope values generally reflect the seasonal patterns delineated by the river and precipitation water isotopes. The slope of soil water line (i.e., $\delta^{2}H$-$\delta^{18}O$ trend) is 7.4, indicating only minor evaporative influences.

We predicted stable isotope values and patterns that we would have observed if the soil carbonate formed only via pedogenesis and if pedogenic carbonate was mixed with detrital carbonate (Figure 6; Figure 7; Figure 8). The mixing model between the stable isotope compositions of detrital and pedogenic carbonate can satisfactorily explain the observed $\delta^{13}C$, $\delta^{18}O$, and Δ_{47} data for all sample types if samples have pedogenic fractions of approximately $0.6 \leq F \leq 1$ (Figure 7). The calculated $\delta^{18}O_{rsw}$ values overlap with the highest observed $\delta^{18}O$ values of precipitation, river, marsh, and soil water isotope values (Figure 5). The environmental conditions required to match the measured $\delta^{13}C_c$ have no or minimal overlap with modern conditions (Figure 8). Only one rhizolith, with the lowest $\delta^{13}C$ value, could potentially be consistent with modern soil conditions.

DISCUSSION

Physical evidence of pedogenic carbonate

The carbonate morphology and underlying sedimentology supports post-glacial, pedogenic carbonate formation (Figure 2). Our initial observations of carbonate morphology are strongly suggestive of *in situ* pedogenic carbonate precipitation (Gile et al., 1966; West et al., 1988b; Gocke and Kuzyakov, 2011; Zamanian et al., 2016) (Figure 2). Calcite rinds indicate *in*

374 *situ* recrystallization of calcite, though they are typically described in deserts (Gile et al., 1966).
375 Rhizoliths cross-cut sedimentary bedding structures and often surround roots of living plants.
376 Filaments of calcite-rich material, called stringers, are also indicative of pedogenic processes.
377 The diffuse carbonate in the matrix throughout the sedimentary sequence is equally likely to be
378 finely-ground detrital limestone or secondary carbonate (Kraimer and Monger, 2009; Li et al.,
379 2013; Zamanian et al., 2021).

380

381 **Isotopic evidence for pedogenic carbonate and its formation processes**

382 We examined the stable isotope data in the context of three scenarios to explain the
383 origin of the soil carbonate: (1) a mixture of pedogenic and detrital carbonate, (2) pedogenic
384 carbonate formed under equilibrium, open-system conditions and (3) pedogenic carbonate
385 formed in closed-system conditions (Figure 6). Each of these scenarios would yield distinct
386 isotope patterns (in $T\Delta_{47}$, $\delta^{18}O$, and $\delta^{13}C$) in the resulting soil carbonate (Figure 6). The isotope
387 and monitoring data are most consistent the scenario that the soil carbonate is a mix between
388 pedogenic and detrital carbonate.

389

390 **A physical mixture of pedogenic and detrital carbonate**

391 A mix between pedogenic and detrital endmembers can parsimoniously explain the
392 observed isotopic values ($\delta^{18}O$, $\delta^{13}C$, $T\Delta_{47}$, and ^{14}C) of the carbonate (Figure 6; Figure 7).
393 Because the $\delta^{18}O$ value of the detrital limestone overlaps with the $\delta^{18}O$ value of pedogenic
394 carbonate formed in equilibrium with modern waters, $\delta^{18}O$ is almost invariant in this scenario
395 (Figure 6), matching the measured $\delta^{18}O_c$/ $\delta^{18}O_{rsw}$values (Figure 5). $T\Delta_{47}$ and $\delta^{13}C$ covary
396 because both are dependent on the mixing fraction (Figure 6). The detrital endmembers

(limestone clasts) have high $T\Delta_{47}$ values of 70-86 °C and high $\delta^{13}C$ values. The sampled rhizolith has a low $T\Delta_{47}$ of 16 °C and a low $\delta^{13}C$ value, while the rinds have intermediate $T\Delta_{47}$ values of 21-33°C and intermediate $\delta^{13}C$ values (Figure 6). Because of this variation, the $T\Delta_{47}$ values provide a strong constraint on the fraction of pedogenic carbonate within the samples ($0.5 \leq F \leq 1$) (Figure 7). A mix between detrital and pedogenic carbonates is also consistent with the radiocarbon ages that predate glacial retreat; the radiocarbon-dead-detrital component would make ^{14}C ages appear older than their true formation age.

The distinctions in stable isotope values with carbonate morphology mostly fit with our expectation given a physical mix. The bulk samples have $\delta^{13}C$ and $\delta^{18}O$ values that overlap with that of the detrital limestone (Fig. 6g-h; Table 2), which is expected given the higher potential for detrital contamination in bulk carbonate. For carbonate morphologies that are more likely to be a higher proportion of pedogenic (rinds, rhizoliths, and stringer), the isotopic composition is explained via a mix of pedogenic and geogenic carbonate (Figure 6; Figure 7). This framework groups rhizoliths, rinds and stringers as having a higher proportion of pedogenic carbonate than bulk samples (Figure 6), as also observed by Zamanian et al., (2021) and Gocke et al. (2011). Using this framework, the isotopic data suggest that the rhizoliths tend to have the higher proportion of pedogenic carbonate than rinds or stringers. This pattern could be a sampling artifact: the rinds were thin (~1 mm) and separating them from carbonate-cemented matrix was subjective. In comparison, the rhizoliths were more straightforward to isolate from matrix because they were thicker (~1 cm), firm, had a predictable, cylindrical geometry, and were whiter than the surrounding matrix. This apparent difference in pedogenic component could be a true result that relates to their formation mechanisms. We might expect rinds to have matrix contamination if they form as hypocoatings in pore space that grows towards the clasts, rather forming gravitationally like a pedothem in arid soils (Ducloux et al., 1984; Durand et al., 2018). In comparison, rhizoliths have been previously shown to be purely secondary (pedogenic) carbonate (Gocke et al., 2011). In one model of rhizolith formation, the first step is that acidic

root exudate dissolves the surrounding matrix (including detrital carbonate and non-carbonate minerals). Subsequently, the root selectively uptakes Ca^{2+} in solution, then rhizolith carbonate precipitates from the remnant Ca^{2+} in solution and CO_2 from microorganism respiration (Barta, 2011; Brazier et al., 2020; Huguet et al., 2021). Therefore, the mixing model can explain the composition and origin of the soil carbonate at the Reserve.

The Monte Carlo mixing model gives predictions for the isotopic composition of the pedogenic carbonate endmembers (Figure 7). The model predicts a range of $\delta^{13}C$ values for the pedogenic carbonate endmember, consistent with formation under mixed C_3-C_4 vegetation regimes or at substantially lower soil CO_2 concentrations than observed today. Our results are therefore consistent with, but do not uniquely identify, a substantial component of C_4 vegetation in southern Michigan in the late deglacial/early Holocene (Nelson et al., 2006; Chapman and Brewer, 2008).

Alternative scenarios: pedogenic carbonate formed in the modern under open- or closed-system conditions

Given that the soil carbonate appears morphologically to be pedogenic, the simplest hypothesis is that the soil carbonate formed via pedogenic processes under post-glacial environmental conditions. However, the isotope data ($\delta^{18}O$, $\delta^{13}C$, $T\Delta_{47}$, and ^{14}C) and monitoring data are not fully compatible with this scenario (Figure 5, Figure 6, Figure 8).

The only evidence that aligns with the pedogenic carbonate scenario is that the $\delta^{18}O_{rsw}$ values overlap with the highest observed $\delta^{18}O$ values of precipitation, river, marsh, and soil water isotope values. This data could be consistent with pedogenic carbonate formation from parent soil waters during the warm half of the year (Figure 5), but the other considered scenarios could also explain the measured $\delta^{18}O_c$ values (Figure 6), so the information from $\delta^{18}O$ is nonunique at this site.

All other isotope data do not match our predictions for open system, modern pedogenic carbonate. First, the radiocarbon ages of 17,366 and 23,691 cal yr BP pre-date glacial retreat from the region (Table 1) (Dalton et al., 2020), which would require pedogenic carbonate formation while the region was covered with an ice sheet. Second, the $T\Delta_{47}$ values of 16 to 33 °C overlap or exceed the maximum measured soil temperatures (25 °C) at 10 to 60 cm (Figure 4). A simple interpretation of this data would suggest pedogenic carbonate formation during the warmest months (but even so, temperatures of 33 °C are not reasonable). This interpretation is inconsistent with the $\delta^{13}C$ modeling that, in a C3-dominated environment, requires formation at pCO_2 ~< 2500 ppm, and the fact that summer pCO_2 exceeds 8000 ppm. Finally, the $\delta^{13}C$ values of the soil carbonate samples are generally inconsistent with predictions of values of pedogenic carbonate formed under modern conditions (colored dots in Figure 8). The $\delta^{13}C$ values of most of the soil carbonate samples are higher than would be expected if they were pedogenic. The environmental conditions capable of recreating the measured soil carbonate $\delta^{13}C$ values are either low soil pCO_2 (~<2500 ppm) or $\delta^{13}C$ values of respired CO_2 of ~-20 to -15 ‰ (colored dots in Figure 8). Neither of these conditions are consistent with modern conditions (black box in Figure 7), where the minimum measured soil pCO_2 is 4000 ppm and the overlying vegetation is dominantly C_3 (forested) (measured $\delta^{13}C_{org}$ ranges from -29.4 ‰ to -24.7 ‰, Jin et al., (2009)). The only samples for which there is some overlap in modeled- and observed- conditions are rhizoliths, which is consistent with stratigraphic evidence supporting that these are primarily modern (Figure 6; Figure 8).

Another possibility is that the rind and bulk samples formed pedogenically immediately after glacial retreat, when the sparse vegetation coverage could lead to high $\delta^{13}C$-CO_2 values in the soil. This possibility could explain their relatively high $\delta^{13}C$ values (Figure 8). However, it is difficult to explain why the post-glacial rinds would have higher formation temperatures than the modern rhizoliths (Table 2; Table 3; Figure 6) given that post-glacial climates are cooler than present-day (c.f., varying seasonality of soil carbonate formation, Kelson et al., 2020).

Furthermore, we might expect that $\delta^{18}O$ of meteoric water and pedogenic carbonate would be different in post-glacial vs. present-day southern Michigan, but we measured uniform $\delta^{18}O$ values amongst the sample types. The mixing model (scenario 1) is a simpler explanation that unifies all the data.

Theoretically, another possibility is that the soil carbonate is forming *in situ*, but rather than following the typical pedogenic model described above, the carbonate is re-precipitated from detrital carbonate in a closed system. Ultimately, this scenario is not consistent with the isotope and monitoring data (Figure 6) and our understanding of shallow vadose zones. In a closed system, meteoric water equilibrates with the gas reservoir and dissolves pre-existing carbonate (i.e., detrital limestone) without further replenishment of CO_2 or water. Jin et al. (2009) report that the vadose zone in the Reserve might be partially closed based on elevated values of $\delta^{13}C$ of DIC at depths > 1.7 m, but those data could also represent equilibrium values at a high pH. A closed system would yield variable $\delta^{13}C$ values and invariant $\delta^{18}O$ values: the $\delta^{13}C$ of carbonate increases with cycles of dissolution and re-precipitation but $\delta^{18}O$ of carbonate retains the $\delta^{18}O$ value derived from meteoric water (Salomons and Mook, 1986; Lohmann, 1988) (Figure 6). This predicted $\delta^{18}O$ vs. $\delta^{13}C$ pattern is displayed by the soil carbonates in the Reserve but could be explained by other scenarios (Figure 6). Closed system precipitation could also explain the "too-old" ^{14}C ages, whereby ^{14}C in the soil pore waters would be partially derived from dissolved limestone and/or pre-glacial, inherited organic matter (Wang et al., 1996). However, under closed system precipitation we would expect uniform clumped isotope temperatures resembling mean annual air temperature at the depths of carbonate formation (> 50 cm) (Quade et al., 2013; c.f., seasonal biases Kelson et al., 2020) (Figure 6). Instead, we document variation in $T\Delta_{47}$ that correlates with $\delta^{13}C$ (Figure 6). Furthermore, under a closed or partially closed system, we might expect an increase in $\delta^{13}C$ with depth, where shallow carbonates form under a more open system. We do not find a depth- $\delta^{13}C$ pattern (Figure 3), though this pattern may be difficult to detect given that we observe distinct carbonate

morphologies with depths (i.e., the deepest carbonates are rhizoliths, which are unlikely to be closed system given their adjacency to roots). Previous workers have shown open system behavior at depths ~< 1 m in soils: even in limestone terrane, pedogenic $\delta^{13}C$ values match predictions of the pedogenic model of mixed atmospheric and respired CO_2 with negligible contribution of CO_2 dissolved from parent limestone (Amundson et al., 1989; Cerling and Quade, 1993). Given these inconsistencies, pedogenic formation in a partially closed vadose zone is unlikely to be the dominant mode of carbonate formation at the Reserve.

Processes driving pedogenic carbonate formation in Southern Michigan and implications for carbon cycling

We can confidently determine that pedogenic carbonate has formed in our field site in southern Michigan, even if it is physically mixed with detrital carbonate, and our data allows us to consider the process(es) driving its formation.

In arid settings, it is thought that pedogenic calcite precipitation is driven by wetting and drying cycles. Infiltrating precipitation dissolves Ca-bearing minerals and brings Ca^{2+} ions (e.g., from dust, Reheis, (2006)) from the surface to depths in the soil profile. When the soil pore water dries via evapotranspiration, it reaches supersaturation with respect to calcite, and calcite precipitates (e.g., Breecker et al., 2009; Tabor et al., 2013; Gallagher and Sheldon, 2016; Huth et al., 2019; Kelson et al., 2023). However, soil drying is probably not the major mechanism driving pedogenic carbonate formation in the Reserve because 1) we observed little variation in soil water content, outside of minor increases that after summer rain (Figure 4) and 2) there is little isotopic evidence of evaporation in the soil waters (Figure 5, Table 4). The $\delta^{18}O$-$\delta^{2}H$ composition of the soil waters falls near the local meteoric water line and has a slope of 7.5 (Table 4); typical soil water evaporation slopes in arid places are 2-3 (Benettin et al., 2018;

526 Bowen et al., 2018). The isotopic composition of the soil waters reflects seasonal patterns of
527 precipitation. For example, we observed wholesale isotope reset to the measured depths of 50
528 cm after precipitation events between 09/03/2021 and 10/28/2021, indicating significant
529 infiltration of unevaporated soil water. In this setting, the formation of pedogenic carbonate is not
530 controlled by a balance between incoming precipitation and soil drying. And, unlike desert
531 settings where carbonate accumulates with time into progressively mature Bk horizons (Gile,
532 1961; Gile et al., 1966), soil carbonate may not be accumulating in the Reserve.
533 Instead, we propose that in the Reserve the pedogenic carbonate is forming ultimately
534 because of an abundant supply of aqueous Ca^{2+} derived from glacially-ground limestone and
535 dolostone in the parent till and seasonal cycles in soil respired CO_2 (Jin et al., 2008a). Fine-
536 grained carbonates, like those ground up by glaciers, are particularly susceptible to dissolution
537 and recrystallization (Anderson et al., 1997; Gallagher and Breecker, 2020). We hypothesize
538 that the detrital limestone is dissolving and re-reprecipitating on a seasonal basis, resulting in
539 pedogenic carbonate formation as an intermediate product (also described by West et al.,
540 1988a). The $^{87}Sr/^{86}Sr$ values of ≈0.709 suggest that the source of Ca^{2+} is marine limestone (or
541 dust derived from marine limestone). In the nearby Huron and Kalamazoo watersheds, Jin et al.
542 (2008a) found that the saturation index of calcite in pore water is constant throughout the year,
543 while the Ca^{2+} concentrations increased during the summer via calcite dissolution at higher
544 pCO_2. In the surface water, lakes, and wetlands, however, secondary calcite precipitates due to
545 degassing (Szramek and Walter, 2004). Our data also show that pCO_2 increases in the
546 summer, probably due to soil respiration. Put together, this evidence suggests that the *in-situ*
547 precipitation of pedogenic carbonate in the soil is driven by cycles of soil respired pCO_2. Higher
548 soil temperatures enable increased respiration, which increases soil pCO_2 and dissolves
549 existing fine-grained calcite while maintaining a constant saturation index. Subsequently,
550 cooling in the fall results in decreased respiration, decreased pCO_2, and decreased Ca^{2+} ions in
551 the pore water as the calcite re-precipitates. This timing and mechanism are consistent with the

552 stable isotope composition of the rhizolith sample that we hypothesize best represents the
553 pedogenic endmember (i.e., the sample with the lowest $\delta^{13}C$ and $T\Delta_{47}$ values). The $T\Delta_{47}$ of the
554 rhizolith is 16 ± 3°C, matching soil temperatures in September to October when pCO_2 is likely
555 decreasing. Our observations support that soil respiration rates, which influence the acid-
556 carrying capacity of soil pore waters, are an important lever in controlling the dissolution and re-
557 precipitation of carbonate in the soil profile, and ultimately the export of bicarbonate to streams
558 (Calmels et al., 2014; Romero-Mujalli et al., 2019).

559 Another factor contributing to pedogenic carbonate formation may be the mixed
560 carbonate mineralogy in the watershed. Dolomite is less soluble and dissolves more slowly than
561 calcite in the temperate climate of Southern Michigan. Groundwaters and surface waters in the
562 Huron River watershed are undersaturated with respected to dolomite ($MgCa(CO_3)_2$) but
563 supersaturated with respect to calcite ($CaCO_3$) (Williams et al., 2007; Jin et al., 2008b).
564 Continued dissolution of dolomite (which releases Ca^{2+} and Mg^{2+}) after soil water is saturated
565 with respect to calcite may contribute to calcite supersaturation in the watershed, setting the
566 stage for calcite re-precipitation.

567 The pedogenic carbonate at the Reserve may represent a geologically transient feature.
568 The carbonate has been leached from the top ~0.5 to 1.5 m at the Reserve after glacial retreat
569 and at similar profiles described in the region (Figure 2; Figure 3) (Jin et al., 2008a, 2009).
570 There is net dissolution of carbonate minerals in the Huron River watershed (Williams et al.,
571 2007; Jin et al., 2008b). It is likely that the observed pedogenic carbonate will ultimately be
572 dissolved and carried away by groundwater on geologic timescales. Thus, the morphology,
573 depth, and amount of pedogenic carbonate in this profile are transient, adjusting to post-glacial
574 conditions. It is unlikely that such soil profiles with chemistry adjusting to changing climate
575 conditions would be preserved in the geologic record as paleosols. If they were preserved,
576 paleosols analogous to those currently found in the Reserve would be poor records of
577 paleoclimate because the stable isotopic composition does not perfectly reflect environmental

conditions in all samples. Even as a transient feature, the pedogenic carbonate represents an important intermediate step in watershed-scale carbonate weathering. The back-precipitation of carbonates in soils could help explain the missing Ca^{2+} in solute chemistry of rivers (Cavazza et al., 1993; Erlanger et al., 2021; Bufe et al., 2022) and could delay the export of bicarbonate from parent material to the ocean.

CONCLUSION

We presented physical and isotopic evidence for pedogenic carbonate formation in the humid, temperate climate of southern Michigan. The isotope values of the soil carbonate are most simply interpreted as a mixture of pedogenic and detrital carbonate. Because of the detrital component in this carbonate-rich glacial drift, paleoclimate reconstructions based on primary pedogenic carbonate material would require finer-scale techniques like laser ablation or secondary ion mass spectrometry (Passey and Cerling, 2006; Oerter et al., 2016; Huth et al., 2020). For hand-drilled samples, it is preferable to avoid limestone terranes when developing soil-based paleoclimate records (Kraimer and Monger, 2009; Sheldon and Tabor, 2009; Cotton and Sheldon, 2012; Michel et al., 2013).

The apparent *in situ* precipitation of rinds and rhizoliths has implications for terrestrial pools of inorganic carbon and carbon cycling. First, this study demonstrates the existence of pedogenic carbonate, at least transiently, in a wider range of ecosystems than is typically recognized (Railsback, 2021; Licht et al., 2022). Though there is net dissolution of carbonates in the glacial till in southern Michigan (Szramek and Walter, 2004), the timescale of dissolution is mediated by open system re-precipitation of calcite in the shallow weathering zone, driven by seasonal fluctuations in soil respired CO_2. Because the formation of pedogenic calcite is likely driven by soil respired CO_2, changes in land use and vegetation cover could affect rates and amount of net calcite precipitation in this setting. Given that much of the Midwest is deeply

mantled in glacial till that may also be rich in finely-ground detrital carbonates, it is possible that re-reprecipitation of pedogenic carbonate may be occurring across much of the landscape. Our results raise the question of how the rates and magnitudes of this calcite re-precipitation mediate the net dissolution of parent limestone and dolomite and thus slow the export of dissolved bicarbonate. If back-precipitation as pedogenic carbonate is occurring on a sufficiently large scale, it could be relevant to considerations of post-glacial chemical weathering rates (Szramek and Walter, 2004), orogen-scale carbonate weathering rates (Erlanger et al., 2021; Bufe et al., 2022), and the efficacy of enhanced weathering in carbonate-rich till (Knapp and Tipper, 2022). Back-precipitation of detrital carbonate as pedogenic carbonate may alter the timing of regional carbon cycling, potentially acting to slow the glacial-enhancement of chemical weathering and attendant CO_2 sequestration that is a negative feedback on climate on medium (~thousand-year) timescales (Sharp et al., 1995; Anderson et al., 2000; Williams et al., 2007), even if it does not alter the geologically long-term (~million year) sequestration (Berner et al., 1983).

ACKNOWLEDGEMENTS

We thank the Edwin S. George Reserve for hosting our research activities, and especially acknowledge Alex Wenner's assistance in removing vegetation and excavating the slope and Nate Sanders as Director at the time of our study. We acknowledge field assistance from Natalie Packard, Margaret Rudnick, Million Mengesha, and Jungpyo Hong. The Ann Arbor precipitation and Huron River water collections were initiated by Phoebe Aron and Alex Thompson and supported by Chris Poulsen. Thanks to Kacey Lohmann and Lora Wingate for performing $\delta^{13}C$ and $\delta^{18}O$ analyses of carbonate. Jack Hutchings assisted with measurements of $\delta^{18}O$ / $\delta^{2}H$ values of water samples. Diego Fernandez assisted with Sr-isotope analysis. We

629 acknowledge funding from the National Science Award Number 2122023 to Levin and Award
630 Number 1854873 to Kelson. This manuscript was improved by comments from Brenden
631 Fischer-Femal, Jeremy Rugenstein, and Associate Editor Kathleen Johnson.

632 Data availability: clumped isotope (Δ_{47}) data at the replicate-level for samples and
633 standards are available from EarthChem (doi: https://doi.org/10.60520/IEDA/113108) and in
634 Supplementary Table S2. Water isotope data will be available at the University of Utah Water
635 Isotope Database upon publication: https://wateriso.utah.edu/waterisotopes/index.html and in
636 Supplementary Table S3.
637

638 **REFERENCES CITED**

639 Amundson R. G., Chadwick O. A., Sowers J. M. and Doner H. E. (1988) Relationship between
640 climate and vegetation and the stable carbon isotope chemistry of soils in the eastern
641 Mojave Desert, Nevada. *Quaternary Research* **29**, 245–254.

642 Amundson R. G., Chadwick O. A., Sowers J. M. and Doner H. E. (1989) The Stable Isotope
643 Chemistry of Pedogenic Carbonates at Kyle Canyon, Nevada. *Soil Science Society of*
644 *America Journal* **53**, 201–210.

645 Anderson N. T., Kelson J. R., Kele S., Daëron M., Bonifacie M., Horita J., Mackey T. J., John C.
646 M., Kluge T., Petschnig P., Jost A. B., Huntington K. W., Bernasconi S. M. and
647 Bergmann K. D. (2021) A Unified Clumped Isotope Thermometer Calibration (0.5–
648 1,100°C) Using Carbonate-Based Standardization. *Geophysical Research Letters* **48**, 1–
649 11.

650 Anderson S. P., Drever J. I., Frost C. D. and Holden P. (2000) Chemical weathering in the
651 foreland of a retreating glacier. *Geochimica et Cosmochimica Acta* **64**, 1173–1189.

652 Anderson S. P., Drever J. I. and Humphrey N. F. (1997) Chemical weathering in glacial
653 environments. *Geology* **25**, 399–402.

654 Arguez A., Durre I., Applequist S., Vose R. S., Squires M. F., Yin X., Heim R. R. and Owen T.
655 W. (2012) NOAA's 1981–2010 U.S. Climate Normals: An Overview. *Bulletin of the*
656 *American Meteorological Society* **93**, 1687–1697.

657 Arkley R. J. (1963) Calculation of carbonate and water movement in soil from climatic data. *Soil*
658 *Science* **96**, 239–248.

659 Aron P. G., Poulsen C. J., Fiorella R. P., Matheny A. M. and Veverica T. J. (2020) An isotopic
660 approach to partition evapotranspiration in a mixed deciduous forest. *Ecohydrology* **13**,
661 1–19.

662 Barta G. (2011) Secondary carbonates in loess-paleosoil sequences: a general review. *Open*
663 *Geosciences* **3**, 129–146.

664 Benettin P., Volkmann T. H. M., Von Freyberg J., Frentress J., Penna D., Dawson T. E. and
665 Kirchner J. W. (2018) Effects of climatic seasonality on the isotopic composition of
666 evaporating soil waters. *Hydrology and Earth System Sciences* **22**, 2881–2890.

667 Bereiter B., Eggleston S., Schmitt J., Nehrbass-Ahles C., Stocker T. F., Fischer H., Kipfstuhl S.
668 and Chappellaz J. (2015) Revision of the EPICA Dome C CO2 record from 800 to 600
669 kyr before present. *Geophysical Research Letters* **42**, 542–549.

670 Bernasconi S. M., Daëron M., Bergmann K. D., Bonifacie M., Meckler A. N., Affek H. P., Bajnai
671 D., Barkan E., Beverly E., Blamart D., Burgener L., Calmels D., Clog M., Davidheiser-
672 Kroll B., Davies A., Dux F., Eiler J., Elliott B., Fetrow C., Fiebig J., Goldberg S., Hermoso
673 M., Huntington K. W., Hyland E., Jaggi M., John C. M., Jost A. B., Katz S., Kelson J.,
674 Kluge T., Kocken I. J., Leutert T. J., Liang D., Lucarelli J., Mackey T. J., Mangenot X.,
675 Meinicke N., Modestou S. E., Müller I. A., Murray S., Neary A., Packard N., Passey B.
676 H., Pelletier E., Piasecki A., Schauer A., Snell K. E., Swart P. K., Tripati A., Upadhyay

677 D., Vennemann T., Winkelstern I., Yarian D., Yoshida N., Zhang N. and Ziegler M.
678 (2021) InterCarb: A community effort to improve inter-laboratory standardization of the
679 carbonate clumped isotope thermometer using carbonate standards. *Geochemistry,*
680 *Geophysics, Geosystems* **22**, e2020GC009588.

681 Berner R. A., Lasaga A. C. and Garrels R. M. (1983) The carbonate-silicate geochemical cycle
682 and its effect on atmospheric carbon dioxide over the past 100 million years. *American*
683 *Journal of Science* **283**, 641–683.

684 Birkeland (1984) *Soils and Geomorphology*., Oxford University Press.

685 Bowen G. J., Putman A., Brooks J. R., Bowling D. R., Oerter E. J. and Good S. P. (2018)
686 Inferring the source of evaporated waters using stable H and O isotopes. *Oecologia* **187**,
687 1025–1039.

688 Brand W., Assonov S. S. and Coplen T. B. (2010) Correction for the 17O interference in δ(13C)
689 measurements when analyzing CO2 with stable isotope mass spectrometry (IUPAC
690 Technical Report). *Pure and Applied Chemistry* **82**, 1719–1733.

691 Brazier J.-M., Schmitt A.-D., Gangloff S., Pelt E., Gocke M. I. and Wiesenberg G. L. B. (2020)
692 Multi-isotope approach (δ44/40Ca, δ88/86Sr and 87Sr/86Sr) provides insights into
693 rhizolith formation mechanisms in terrestrial sediments of Nussloch (Germany).
694 *Chemical Geology* **545**, 119641.

695 Breecker D. O., Sharp Z. D. and McFadden L. D. (2009) Seasonal bias in the formation and
696 stable isotopic composition of pedogenic carbonate in modern soils from central New
697 Mexico, USA. *Bulletin of the Geological Society of America* **121**, 630–640.

698 Bufe A., Cook K. L., Galy A., Wittmann H. and Hovius N. (2022) The effect of lithology on the
699 relationship between denudation rate and chemical weathering pathways – evidence
700 from the eastern Tibetan Plateau. *Earth Surface Dynamics* **10**, 513–530.

701 Calmels D., Gaillardet J. and François L. (2014) Sensitivity of carbonate weathering to soil CO2
702 production by biological activity along a temperate climate transect. *Chemical Geology*
703 **390**, 74–86.

704 Cavazza W., Zuffa G. G., Camporesi C. and Ferretti C. (1993) Sedimentary recycling in a
705 temperate climate drainage basin (Senio River, north-central Italy): Composition of
706 source rock, soil profiles, and fluvial deposits. In *Geological Society of America Special*
707 *Papers* Geological Society of America. pp. 247–262.

708 Cerling T. E. (1984) The stable isotopic composition of modern soil carbonate and its relation to
709 climate. *Earth Planetary Science Letters* **71**, 229-240.

710 Cerling T. E. and Quade J. (1993) Stable carbon and oxygen isotopes in soil carbonates.
711 *Geophysical Monograph* **78**, 217–231.

712 Chapman K. A. and Brewer R. (2008) Prairie and Savanna in Southern Lower Michigan:
713 History, classification, ecology. *The Michigan Botanist* **47**.

714 Comer P. J., Albert D. A., Wells H. A., Hart, B. L., Raab J. B., Price D. L., Kashian D. M. and
715 Corner, R. A. (1995) Michigan's Presettlement Vegetation, as Interpreted from the
716 General Land Office Surveys 1816-1856. *Michigan Natural Features Inventory, Lansing,*
717 *MI. digital map.*

718 Coplen T. B. (2007) Calibration of the calcite–water oxygen-isotope geothermometer at Devils
719 Hole, Nevada, a natural laboratory. *Geochimica et Cosmochimica Acta* **71**, 3948–3957.

720 Cotton J. M. and Sheldon N. D. (2012) New constraints on using paleosols to reconstruct
721 atmospheric pCO2. *Bulletin of the Geological Society of America* **124**, 1411–1423.

722 Daëron M. (2021) Full Propagation of Analytical Uncertainties in Δ47 Measurements.
723 *Geochemistry, Geophysics, Geosystems* **22**, e2020GC009592.

724 Daëron M., Blamart D., Peral M. and Affek H. P. (2016) Absolute isotopic abundance ratios and
725 the accuracy of Δ47 measurements. *Chemical Geology* **442**, 83–96.

726 Dalton A. S., Margold M., Stokes C. R., Tarasov L., Dyke A. S., Adams R. S., Allard S., Arends
727 H. E., Atkinson N., Attig J. W., Barnett P. J., Barnett R. L., Batterson M., Bernatchez P.,
728 Borns H. W., Breckenridge A., Briner J. P., Brouard E., Campbell J. E., Carlson A. E.,
729 Clague J. J., Curry B. B., Daigneault R.-A., Dubé-Loubert H., Easterbrook D. J., Franzi
730 D. A., Friedrich H. G., Funder S., Gauthier M. S., Gowan A. S., Harris K. L., Hétu B.,
731 Hooyer T. S., Jennings C. E., Johnson M. D., Kehew A. E., Kelley S. E., Kerr D., King E.
732 L., Kjeldsen K. K., Knaeble A. R., Lajeunesse P., Lakeman T. R., Lamothe M., Larson
733 P., Lavoie M., Loope H. M., Lowell T. V., Lusardi B. A., Manz L., McMartin I., Nixon F.
734 C., Occhietti S., Parkhill M. A., Piper D. J. W., Pronk A. G., Richard P. J. H., Ridge J. C.,
735 Ross M., Roy M., Seaman A., Shaw J., Stea R. R., Teller J. T., Thompson W. B.,
736 Thorleifson L. H., Utting D. J., Veillette J. J., Ward B. C., Weddle T. K. and Wright H. E.
737 (2020) An updated radiocarbon-based ice margin chronology for the last deglaciation of
738 the North American Ice Sheet Complex. *Quaternary Science Reviews* **234**, 106223.

739 D'Avello T. P., Waltman W. J., Waltman S. W., Thompson J. A. and Brennan J. (2019)
740 Revisiting the Pedocal/Pedalfer boundary and Soil Moisture Regimes using the
741 javaNewhall simulation model and PRISM data. *Geoderma* **353**, 125–132.

742 Davidson G. R. (1995) The stable isotopic composition and measurement of carbon in soil CO2.
743 *Geochimica et Cosmochimica Acta* **59**, 2485–2489.

744 Ducloux J., Butel P. and Dupuis T. (1984) Microséquence minéralogique des carbonates de
745 calcium dans une accumulation carbonatée sous galets calcaires, dans l'Ouest de la
746 France. *Pédologie (Gent)*, 161–177.

747 Durand N., Monger H. C., Canti M. G. and Verrecchia E. P. (2018) Calcium Carbonate
748 Features. In *Interpretation of Micromorphological Features of Soils and Regoliths*
749 Elsevier. pp. 205–258.

750 Eggleston S., Schmitt J., Bereiter B., Schneider R. and Fischer H. (2016) Evolution of the stable
751 carbon isotope composition of atmospheric CO2 over the last glacial cycle.
752 *Paleoceanography* **31**, 434–452.

753 Eiler J. M. (2007) “Clumped-isotope” geochemistry—The study of naturally-occurring, multiply-
754 substituted isotopologues. *Earth and Planetary Science Letters* **262**, 309–327.

755 Erlanger E. D., Rugenstein J. K. C., Bufe A., Picotti V. and Willett S. D. (2021) Controls on
756 Physical and Chemical Denudation in a Mixed Carbonate-Siliciclastic Orogen. *Journal of*
757 *Geophysical Research: Earth Surface* **126**, e2021JF006064.

758 Eswaran H., Reich F. P., Kimble J. M., Beinroth F. H., Padamnabhan E. and Monchareon P.
759 (2000) Global Carbon Stocks. In *Global Climate Change and Pedogenic Carbonates*
760 (eds. R. Lal, J. M. Kimnble, H. Eswaran, and B. A. Stewart). CRC Press, Boca Raton,
761 FL.

762 Farrand W. R. and Bell D. R. (1982) Quaternary Geology of Southern Michigan. In *Geological*
763 *Publication QG-01, Quaternary Geology of Michigan* Michigan Department of Natural
764 Resources.

765 Ferdush J. and Paul V. (2021) A review on the possible factors influencing soil inorganic carbon
766 under elevated CO2. *Catena* **204**, 105434.

767 Gallagher T. M. and Breecker D. O. (2020) The Obscuring Effects of Calcite Dissolution and
768 Formation on Quantifying Soil Respiration. *Global Biogeochemical Cycles* **34**, 0–3.

769 Gallagher T. M. and Sheldon N. D. (2016) Combining soil water balance and clumped isotopes
770 to understand the nature and timing of pedogenic carbonate formation. *Chemical*
771 *Geology* **435**, 79–91.

772 Gile L. H. (1961) A Classification of ca Horizons in Soils of a Desert Region, Dona Ana County,
773 New Mexico. *Soil Science Society of America Journal* **25**, 52–61.

774 Gile L. H., Peterson F. F. and Grossman R. B. (1966) Morphological and Genetic Sequences of
775 Carbonate Accumulation in Desert Soils. *Soil Science* **101**, 347–360.

776 Gocke M. and Kuzyakov Y. (2011) Effect of temperature and rhizosphere processes on
777 pedogenic carbonate recrystallization: Relevance for paleoenvironmental applications.
778 *Geoderma* **166**, 57–65.

779 Gocke M., Pustovoytov K., Kühn P., Wiesenberg G. L. B., Löscher M. and Kuzyakov Y. (2011)
780 Carbonate rhizoliths in loess and their implications for paleoenvironmental reconstruction
781 revealed by isotopic composition: δ13C, 14C. *Chemical Geology* **283**, 251–260.

782 Gröning M., Lutz H. O., Roller-Lutz Z., Kralik M., Gourcy L. and Pöltenstein L. (2012) A simple
783 rain collector preventing water re-evaporation dedicated for δ18O and δ2H analysis of
784 cumulative precipitation samples. *Journal of Hydrology* **448–449**, 195–200.

785 Huguet A., Bernard S., El Khatib R., Gocke M. I., Wiesenberg G. L. B. and Derenne S. (2021)
786 Multiple stages of plant root calcification deciphered by chemical and
787 micromorphological analyses. *Geobiology* **19**, 75–86.

788 Huntington K. W. and Petersen S. V. (2023) Frontiers of carbonate clumped isotope
789 thermometry. *Annual Review of Earth and Planetary Sciences* **51**.

790 Hutchings J. A. and Konecky B. L. (2023) Optimization of a Picarro L2140-i cavity ring-down
791 spectrometer for routine measurement of triple oxygen isotope ratios in meteoric waters.
792 *Atmospheric Measurement Techniques* **16**, 1663–1682.

793 Huth T. E., Cerling T. E., Marchetti D. W., Bowling D. R., Ellwein A. L. and Passey B. H. (2019)
794 Seasonal bias in soil carbonate formation and its implications for interpreting high-
795 resolution paleoarchives: evidence from southern Utah. *Journal of Geophysical*
796 *Research: Biogeosciences* **124**, 616–632.

797 Huth T. E., Cerling T. E., Marchetti D. W., Bowling D. R., Ellwein A. L., Passey B. H., Fernandez
798 D. P., Valley J. W. and Orland I. J. (2020) Laminated soil carbonate rinds as a
799 paleoclimate archive of the Colorado Plateau. *Geochimica et Cosmochimica Acta* **282**,
800 227–244.

801 Jin L., Hamilton S. K. and Walter L. M. (2008a) Mineral weathering rates in glacial drift soils (SW
802 Michigan, USA): New constraints from seasonal sampling of waters and gases at soil
803 monoliths. *Chemical Geology* **249**, 129–154.

804 Jin L., Ogrinc N., Hamilton S. K., Szramek K., Kanduc T. and Walter L. M. (2009) Inorganic
805 carbon isotope systematics in soil profiles undergoing silicate and carbonate weathering
806 (Southern Michigan, USA). *Chemical Geology* **264**, 139–153.

807 Jin L., Williams E. L., Szramek K. J., Walter L. M. and Hamilton S. K. (2008b) Silicate and
808 carbonate mineral weathering in soil profiles developed on Pleistocene glacial drift
809 (Michigan, USA): Mass balances based on soil water geochemistry. *Geochimica et*
810 *Cosmochimica Acta* **72**, 1027–1042.

811 Kelson J. R., Huntington K. W., Breecker D. O., Burgener L. K., Gallagher T. M., Hoke G. D.
812 and Petersen S. V. (2020) A proxy for all seasons? A synthesis of clumped isotope data
813 from Holocene soil carbonates. *Quaternary Science Reviews* **234**, 106259.

814 Kelson J. R., Huth T. E., Passey B. H., Levin N. E., Petersen S. V., Ballato P., Beverly E. J.,
815 Breecker D. O., Hoke G. D., Hudson A. M., Ji H., Licht A., Oerter E. J. and Quade J.
816 (2023) Triple oxygen isotope compositions of globally distributed soil carbonates record
817 widespread evaporation of soil waters. *Geochimica et Cosmochimica Acta* **355**, 138–
818 160.

819 Kim S. T. and O'Neil J. R. (1997) Equilibrium and nonequilibrium oxygen isotope effects in
820 synthetic carbonates. *Geochimica et Cosmochimica Acta* **61**, 3461–3475.

821 Knapp W. J. and Tipper E. T. (2022) The efficacy of enhancing carbonate weathering for carbon
822 dioxide sequestration. *Frontiers in Climate* **4**.

823 Kraimer R. A. and Monger H. C. (2009) Carbon isotopic subsets of soil carbonate-A particle size
824 comparison of limestone and igneous parent materials. *Geoderma* **150**, 1–9.

825 Li G., Chen J. and Chen Y. (2013) Primary and secondary carbonate in Chinese loess
826 discriminated by trace element composition. *Geochimica et Cosmochimica Acta* **103**,
827 26–35.

828 Licht A., Kelson J., Bergel S., Schauer A., Petersen S. V., Capirala A., Huntington K. W.,
829 Dupont-Nivet G., Win Z. and Aung D. W. (2022) Dynamics of Pedogenic Carbonate
830 Growth in the Tropical Domain of Myanmar. *Geochemistry, Geophysics, Geosystems*
831 **23**, e2021GC009929.

832 Lohmann K. C. (1988) Geochemical patterns of meteoric diagenetic systems and their
833 applications to studies of paleokarst. In *Paleokarst* (eds. N. P. James and P. W.
834 Choquette). Springer New York, New York. pp. 58–80.

835 Michel L. A., Driese S. G., Nordt L. C., Breecker D. O., Labotka D. M. and Dworkin S. I. (2013)
836 Stable-Isotope Geochemistry of Vertisols Formed On Marine Limestone and Implications
837 for Deep-Time Paleoenvironmental Reconstructions. *Journal of Sedimentary Research*
838 **83**, 300–308.

839 Milstein R. L. (1987) Bedrock Geology of Southern Michigan.

840 Monger H. C., Kraimer R. A., Khresat S., Cole D. R., Wang X. and Wang J. (2015)
841 Sequestration of inorganic carbon in soil and groundwater. *Geology* **43**, 375–378.

842 Naorem A., Jayaraman S., Dalal R. C., Patra A., Rao C. S. and Lal R. (2022) Soil Inorganic
843 Carbon as a Potential Sink in Carbon Storage in Dryland Soils—A Review. *Agriculture*
844 **12**, 1256.

845 Nelson D. M., Hu F. S., Grimm E. C., Curry B. B. and Slate J. E. (2006) The influence of aridity
846 and fire on Holocene prairie communities in the Eastern Prairie Peninsula. *Ecology* **87**,
847 2523–2536.

848 Nyachoti S., Jin L., Tweedie C. E. and Ma L. (2019) Insight into factors controlling formation
849 rates of pedogenic carbonates: A combined geochemical and isotopic approach in
850 dryland soils of the US Southwest. *Chemical Geology* **527**, 118503.

851 Oerter E. J., Sharp W. D., Oster J. L., Ebeling A., Valley J. W., Kozdon R., Orland I. J.,
852 Hellstrom J., Woodhead J. D., Hergt J. M., Chadwick O. A. and Amundson R. (2016)
853 Pedothem carbonates reveal anomalous North American atmospheric circulation
854 70,000-55,000 years ago. *Proceedings of the National Academy of Sciences of the*
855 *United States of America* **113**, 919–924.

856 Passey B. H. and Cerling T. E. (2006) In situ stable isotope analysis (δ13C, δ18O) of very small
857 teeth using laser ablation GC/IRMS. *Chemical Geology* **235**, 238–249.

858 Pelletier E. M. (2020) Variability of Meteoric Water Isotopes in the Great Lakes Region.
859 Undergraduate Honors Thesis, University of Michigan, Ann Arbor.

860 Pfeiffer M., Padarian J. and Vega M. P. (2023) Soil inorganic carbon distribution, stocks and
861 environmental thresholds along a major climatic gradient. *Geoderma* **433**, 116449.

862 Plaza C., Zaccone C., Sawicka K., Méndez A. M., Tarquis A., Gascó G., Heuvelink G. B. M.,
863 Schuur E. A. G. and Maestre F. T. (2018) Soil resources and element stocks in drylands
864 to face global issues. *Scientific Reports* **8**, 13788.

865 Putman A. L., Fiorella R. P., Bowen G. J. and Cai Z. (2019) A global perspective on local
866 meteoric water lines: Meta-analytic insight into fundamental controls and practical
867 constraints. *Water Resources Research* **55**, 6896–6910.

868 Quade J., Eiler J. M., Daëron M. and Achyuthan H. (2013) The clumped isotope
869 geothermometer in soil and paleosol carbonate. *Geochimica et Cosmochimica Acta* **105**.

870 Railsback L. B. (2021) Pedogenic carbonate nodules from a forested region of humid climate in
871 central Tennessee, USA, and their implications for interpretation of C3 -C4 relationships
872 and seasonality of meteoric precipitation from carbon isotope (δ13C) data. *Catena* **200**,
873 1–8.

874 Reheis M. C. (2006) A 16-year record of eolian dust in Southern Nevada and California, USA:
875 Controls on dust generation and accumulation. *Journal of Arid Environments* **67**, 487–
876 520.

877 Reimer P. J., Baillie M. G. L., Bard E., Bayliss A., Beck J. W., Blackwell P. G., Ramsey C. B.,
878 Buck C. E., Burr G. S., Edwards R. L., Friedrich M., Grootes P. M., Guilderson T. P.,
879 Hajdas I., Heaton T. J., Hogg A. G., Hughen K. A., Kaiser K. F., Kromer B., McCormac
880 F. G., Manning S. W., Reimer R. W., Richards D. A., Southon J. R., Talamo S., Turney
881 C. S. M., Plicht J. van der and Weyhenmeyer C. E. (2009) IntCal09 and Marine09
882 Radiocarbon Age Calibration Curves, 0–50,000 Years cal BP. *Radiocarbon* **51**, 1111–
883 1150.

884 Retallack G. J. (2005) Pedogenic carbonate proxies for amount and seasonality of precipitation
885 in paleosols. *Geology* **33**, 333–336.

886 Rieck R. L. (1976) The glacial geomorphology of an interlobate area in southeast Michigan:
887 relationships between landforms, sediments, and bedrock. PhD, Michigan State
888 University.

889 Roller N. E. G. (1974) *Airphoto mapping of ecosystem development on the Edwin S. George*
890 *Reserve*., School of Natural Resources, University of Michigan, Ann Arbor, MI.

891 Romanek C. S., Grossman E. L. and Morse J. W. (1992) Carbon isotopic fractionation in
892 synthetic aragonite and calcite: Effects of temperature and precipitation rate.
893 *Geochimica et Cosmochimica Acta* **56**, 419–430.

894 Romero-Mujalli G., Hartmann J. and Börker J. (2019) Temperature and CO2 dependency of
895 global carbonate weathering fluxes – Implications for future carbonate weathering
896 research. *Chemical Geology* **527**, 118874.

897 Royer D. L. (1999) Depth to pedogenic carbonate horizon as a paleoprecipitation indicator?
898 *Geology* **27**, 1123–1126.

899 Salomons W. and Mook W. G. (1986) Isotope Geochemistry of Carbonates in the Weathering
900 Zone. In *Handbook of Environmental Isotope Geochemistry, Vol. 2., The Terrestrial*
901 *Environment* (eds. P. Fritz and J. Ch. Fonts). Elsevier B.V., Amsterdam. pp. 239–269.

902 Schaetzl R. J. (2001) Late Pleistocene Ice-Flow Directions and the Age of Glacial Landscapes
903 in Northern Lower Michigan. *Physical Geography* **22**, 28–41.

Schaetzl R. J. (1992) Texture, Mineralogy, and Lamellae Development in Sandy Soils in Michigan. *Soil Science Society of America Journal* **56**, 1538–1545.

Schauer A. J., Kelson J. R., Saenger C. and Huntington K. W. (2016) Choice of 17O correction affects clumped isotope (Δ47) values of CO2 measured with mass spectrometry. *Rapid Communications in Mass Spectrometry* **30**, 2607–2616.

Sharififar A., Minasny B., Arrouays D., Boulonne L., Chevallier T., Van Deventer P., Field D. J., Gomez C., Jang H.-J., Jeon S.-H., Koch J., McBratney A. B., Malone B. P., Marchant B. P., Martin M. P., Monger C., Munera-Echeverri J.-L., Padarian J., Pfeiffer M., Richer-de-Forges A. C., Saby N. P. A., Singh K., Song X.-D., Zamanian K., Zhang G.-L. and Van Zijl G. (2023) Soil inorganic carbon, the other and equally important soil carbon pool: Distribution, controlling factors, and the impact of climate change. In *Advances in Agronomy* Elsevier. pp. 165–231.

Sharp M., Tranter M., Brown G. H. and Skidmore M. (1995) Rates of chemical denudation and CO2 drawdown in a glacier-covered alpine catchment. *Geology* **23**, 61–64.

Sheldon N. D. and Tabor N. J. (2009) Quantitative paleoenvironmental and paleoclimatic reconstruction using paleosols. *Earth-Science Reviews* **95**, 1–52.

Slessarev E. W., Lin Y., Bingham N. L., Johnson J. E., Dai Y., Schimel J. P. and Chadwick O. A. (2016) Water balance creates a threshold in soil pH at the global scale. *Nature* **540**, 567–569.

Stanbery C. A., Pierce J. L., Benner S. G. and Lohse K. (2017) On the rocks: Quantifying storage of inorganic soil carbon on gravels and determining pedon-scale variability. *Catena* **157**, 436–442.

Stanbery C., Ghahremani Z., Huber D. P., Will R., Benner S. G., Glenn N., Hanif T., Spaete L., Terhaar D., Lohse K. A., Seyfried M., Freutel W. and Pierce J. L. (2023) Controls on the presence and storage of soil inorganic carbon in a semi-arid watershed. *Catena* **225**, 106980.

Steiger R. H. and Jäger E. (1977) Subcommission on geochronology: Convention on the use of decay constants in geo- and cosmochronology. *Earth and Planetary Science Letters* **36**, 359–362.

Strong G. E., Giles J. R. A. and Wright V. P. (1992) A Holocene calcrete from North Yorkshire, England: implications for interpreting palaeoclimates using calcretes. *Sedimentology* **39**, 333–347.

Stuiver M. and Reimer P. J. (1993) Extended 14C Data Base and Revised CALIB 3.0 14C Age Calibration Program. *Radiocarbon* **35**, 215–230.

Szramek K. and Walter L. M. (2004) Impact of Carbonate Precipitation on Riverine Inorganic Carbon Mass Transport from a Mid-continent, Forested Watershed. *Aquatic Geochemistry* **10**, 99–137.

Tabor N. J., Myers T. S., Gulbranson E., Rasmussen C. and Sheldon N. D. (2013) Carbon Stable Isotope Composition of Modern Calcareous Soil Profiles in California:

Implications for CO2 Reconstructions from Calcareous Paleosols. In *New Frontiers in Paleopedology and Terrestrial Paleoclimatology: Paleosols and Soil Surface Analog Systems* (ed. S. G. Driese). SEPM (Society for Sedimentary Geology). pp. 17–34.

Tipple B. J. and Pagani M. (2007) The Early Origins of Terrestrial C $_4$ Photosynthesis. *Annual Review of Earth and Planetary Sciences* **35**, 435–461.

United States Department of Agriculture, Natural Resources Conservation Service (2022) *Land Resource Regions and Major Land Resource Areas of the United States, the Caribbean, and the Pacific Basin*., United States Department of Agriculture, Natural Resources Conservation Service.

Veizer J., Ala D., Azmy K., Bruckschen P., Buhl D., Bruhn F., Garden G. A. F., Diener A., Ebneth S., Godderis Y., Jasper T., Korte C., Pawellek F., Podlaha O. G. and Strauss H. (1999) 87Sr/86Sr, δ13C and δ18O evolution of Phanerozoic seawater. *Chemical Geology* **161**, 59–88.

Wang Y., Cerling T. E. and Effland W. R. (1993) Stable isotope ratios of soil carbonate and soil organic matter as indicators of forest invasion of prairie near Ames, Iowa. *Oecologia* **95**, 365–369.

Wang Y., McDonald E. V., Amundson R. G., McFadden L. D. and Chadwick O. A. (1996) An isotopic study of soils in chronological sequences of alluvial deposits, Providence Mountains, California. *Geological Society Of America Bulletin* **108**, 379–391.

Wani O. A., Kumar S. S., Hussain N., Wani A. I. A., Babu S., Alam P., Rashid M., Popescu S. M. and Mansoor S. (2023) Multi-scale processes influencing global carbon storage and land-carbon-climate nexus: A critical review. *Pedosphere* **33**, 250–267.

West A. G., Patrickson S. J. and Ehleringer J. R. (2006) Water extraction times for plant and soil materials used in stable isotope analysis. *Rapid Communications in Mass Spectrometry* **20**, 1317–1321.

West L. T., Drees L. R., Wilding L. P. and Rabenhorst M. C. (1988a) Differentiation of pedogenic and lithogenic carbonate forms in Texas. *Geoderma* **43**, 271–287.

West L. T., Wilding L. P. and Hallmark C. T. (1988b) Calciustolls in Central Texas: II. Genesis of Calcic and Petrocalcic Horizons. *Soil Science Society of America Journal* **52**, 1731–1740.

White J. H. and Defliese W. F. (2023) δ13C and δ18O heterogeneities in carbonates: Nonlinear mixing in the application of dual-carbonate-clumped isotope thermometer. *Rapid Communications in Mass Spectrometry* **37**, e9627.

Williams E. L., Szramek K. J., Jin L., Ku T. C. W. and Walter L. M. (2007) The carbonate system geochemistry of shallow groundwater–surface water systems in temperate glaciated watersheds (Michigan, USA): Significance of open-system dolomite weathering. *The Geological Society of America Bulletin* **119**, 515–528.

Zamanian K., Lechler A. R., Schauer A. J., Kuzyakov Y. and Huntington K. W. (2021) The δ13C, δ18O and Δ47 records in biogenic, pedogenic and geogenic carbonate types from

paleosol-loess sequence and their paleoenvironmental meaning. *Quaternary Research* **101**, 256–272.

Zamanian K., Pustovoytov K. and Kuzyakov Y. (2016) Pedogenic carbonates: Forms and formation processes. *Earth-Science Reviews* **157**, 1–17.

Zhou J. and Chafetz H. S. (2010) Pedogenic Carbonates in Texas: Stable-Isotope Distributions and Their Implications for Reconstructing Region-Wide Paleoenvironments. *Journal of Sedimentary Research* **80**, 137–150.

991 **LIST OF TABLES**

992 Table 1: Radiocarbon and strontium isotope data for soil carbonates from the Reserve

993 Table 2: Stable carbon and oxygen isotope data from carbonates in the Reserve

994 Table 3: Clumped isotope (Δ_{47}) data and calculated $\delta^{18}O_{rsw}$ values for select soil carbonates

995 from the Reserve

996 Table 4: Summary of Meteoric and Soil Water Isotope ($\delta^{18}O$, $\delta^{2}H$) Data

997

LIST OF FIGURES

Figure 1: Regional map showing the position of the Edwin S George Reserve (ESGR) (red star) relative to the cities of Ann Arbor and Lansing, Michigan, with the US state border in black (WGS84 datum used). The inset shows the position of the site in North America.

Figure 2: Overview of the study site and soil carbonate morphologies. A) Photo of the excavated cut slope of the knoll with overlaid interpretational sketch. B) Photograph of the soil horizons developed on the uppermost gravel unit 9 (see description in Figure 3. Orange flags are spaced 20 cm apart. C) Stringer (filaments) and a rhizolith at 90 cm depth. D) Rhizolith encasing a root at 270 cm depth. E) Carbonate rind coating a clast. This clast was found in the float at the base of the excavated knoll. Rinds on the undersides of clasts were found *in situ* at 40 cm and below. F) Rinds coating clasts and diffuse carbonate in the matrix of the lower gravel unit (depths of 325-400 cm). Pencil for scale.

Figure 3: Site stratigraphy and soil carbonate stable isotope values. A) Sedimentary composition and pedogenic features described on the excavated, cut slope of the knoll. B) Stable isotope values ($\delta^{13}C$ and $\delta^{18}O$) of soil and detrital carbonate samples that were collected from the excavated slope of the knoll and in soil pits dug from the top of the knoll (depth to carbonate differed by 20-40 cm between those locations). Lines connect data points of the same carbonate type.

Figure 4 Below-ground soil monitoring data and precipitation data. A) Soil temperature measured at depths of 10, 30 and 60 cm (lines). Colored horizontal stripes indicate $T\Delta_{47}$ values (± 1 SE) for soil carbonate samples with Δ_{47} data (20ESGR-50, 20ESGR-slope-120, 20ESGR70-75,22ESGR-rhizo180). B) Soil water content at the site. C) Daily total precipitation from nearby NOAA weather station US1MIWS0055 42.43423, -83.68679), accessed via Climate

Data Online (https://www.ncei.noaa.gov/cdo-web/). D) Soil CO_2 concentrations measured at 60 cm only. The sensor used maxes out at 10,000 ppm; summertime pCO_2 values exceed the maximum.

Figure 5. Stable isotope values ($\delta^{18}O$, $\delta^{2}H$) of surface and soil waters from southern Michigan and reconstructed soil waters ($\delta^{18}O_{rsw}$) from soil carbonates a) $\delta^{18}O$ - $\delta^{2}H$ relationships for meteoric waters and soil waters. The local meteoric water line (LMWL) is calculated from precipitation data. b) $\delta^{18}O$-*d*-excess values for of all water types. c) Box plots of $\delta^{18}O$ values of water, soil water, and reconstructed soil water. d) $\delta^{18}O$ throughout the collection period. Horizontal colored stripes (orange, red, gold, yellow) indicate the $\delta^{18}O_{rsw}$ values for soil carbonate samples with $T\Delta_{47}$ data (note that 20ESGR-slope-70-75 (gold) and 22ESGR-rhizolith-180cm (yellow) have overlapping values) and their relationship with warm season meteoric water samples.

Figure 6. Expected and measured isotope patterns for three scenarios explaining the origin of the soil carbonate. Scenario 1 (a and b): A physical mixture between pedogenic and detrital carbonate. In this scenario, $\delta^{13}C$ and $T\Delta_{47}$ vary with the fraction included detrital material. $\delta^{18}O$ is uniform because $\delta^{18}O$ of carbonate formed in equilibrium with meteoric waters is similar to (within 1-2 ‰ of) the $\delta^{18}O$ values of detrital carbonates. Scenario 2 (c and d): Pedogenic carbonate in an open system. In this scenario, soil carbonate has a relatively small range of $\delta^{18}O$, $\delta^{13}C$, and $T\Delta_{47}$ values that reflects isotopic equilibrium with the environment during a single season. Scenario 3 (e and f): Pedogenic carbonate in a closed system with respect to soil CO_2. In this scenario, $\delta^{13}C$ varies while $\delta^{18}O$ and $T\Delta_{47}$ are constant. Measured stable isotope values of the distinct carbonate types from the Reserve (g and h). One example of a mixing line calculated between a set of potential pedogenic and detrital endmembers is shown with black lines and arrows (i.e., one iteration of scenario a). Possible ranges of pedogenic and detrital

endmember compositions at the Reserve are shown as rectangles outlined in black, filled in green and purple, respectively. These ranges are only illustrative and differ from the ranges used to constrain the mixing model shown (Figure 8). The illustrated possible ranges of the pedogenic endmember $\delta^{13}C$ values are calculated based on $\delta^{13}C$-CO_2 values measured in the Huron River watershed (Jin et al., 2009). The illustrated range of the pedogenic endmember $\delta^{18}O$ values is based on Huron River waters and carbonate growth temperature of 15°C. The possible range in $\delta^{18}O$ and $\delta^{13}C$ values of the limestone endmember is based on secular trends from Vezier et al. (1999) and measured limestone clast values. Where error bars are not visible, they are smaller than symbol size. The slight curvature in the $\delta^{13}C$-TΔ_{47} mixing line is due to nonlinearity in the relationship between temperature and Δ_{47}.

Figure 7. Solutions for the model of two-component mixing between detrital and pedogenic carbonate. Plots show solutions for carbonate in sample groups separated as rinds (a and c) and rhizoliths or stringers (b and d) in $\delta^{13}C$-$\delta^{18}O$ and $\delta^{13}C$-TΔ_{47} space. We only modeled samples with $\delta^{13}C$, $\delta^{18}O$, and Δ_{47} data to provide maximum constraint on solutions for *F*. The dark gray box outlines the possible detrital endmember values, the light gray box outlines the full range of possible pedogenic carbonate endmember values on a global basis, and the red triangles are observed sample values. The small colored dots are the feasible pedogenic carbonate endmembers that can mix with the detrital endmember to create the observed soil carbonate isotope composition at the assigned fraction of pedogenic carbonate (*F*). Different colors denote mixing model solutions for different samples. For visual clarity, we show simulations in 10% increments of the fraction of pedogenic carbonate; the large circles are averages for each increment and lines connect the average values. The set of endmember solutions for the assumed fraction of pedogenic carbonate are only labeled for the bottom right sample in each panel (e.g., “solutions for *F*=0.6”), but all samples have the same pattern. Note

1076 that when the assumed fraction of pedogenic carbonate is 100% (*F*=1), the endmember
1077 solutions necessarily match the observed sample isotope composition.
1078
1079 **Figure 8.** Environmental conditions capable of creating observed soil carbonate $\delta^{13}C$ values
1080 assuming samples are pedogenic carbonate formed in an open system. Theoretically feasible
1081 conditions for the $\delta^{13}C$ of soil respiration and soil CO_2 concentration are shown for three sample
1082 groups: (a) rinds, (b) rhizoliths and stringers, and (c) bulk soil samples. Colored dots denote
1083 solution spaces (10,000 iterations each) for different samples. Solutions that are consistent with
1084 modern conditions must fall within the black box, which outlines modern conditions for $\delta^{13}C$ of
1085 soil respiration in a C_3 dominated landscape (Tipple and Pagani, 2007; Jin et al., 2009) and the
1086 observed soil CO_2 concentrations during our monitoring period.
1087

Table 1: Radiocarbon and strontium isotope data for soil carbonates from the Reserve

Sample ID	Carbonate morphology	Median ^{14}C ages calibrated using Calib. Rev. 8	^{14}C age error (1-sigma, yr BP)	$^{87}Sr/^{86}Sr$
20ESGR-50cm	rind	23,691 cal yr BP	100	0.709693
20ESGR-70-75cm	rind	17,366 cal yr BP	79	0.709461

Table 2: Stable carbon and oxygen isotope values of carbonates from the Reserve

Sample ID	Depth (cm)	Carbonate Morphology	$\delta^{13}C_c$ ‰ VPDB [a]	$\delta^{18}O_c$ ‰ VPDB [a]
20EGSR-50	-50	rind	-3.2	-7.3
20EGSR-55-60	-55	rind	-3.2	-6.2
20EGSR-slope-60-1	-60	rind	-5.6	-8.0
20EGSR-slope-60-2	-60	rind	-4.9	-7.9
20EGSR-slope-70-75	-70	rind	-3.0	-7.4
20EGSR-slope-100-105	-100	rind	-5.7	-8.3
20EGSR-slope-120	-120	rind	-5.1	-8.0
22ESGR-whitestripe-200to220cm	-210	white matrix in bulk soil	-2.5	-6.6
22ESGR-rhizolith-180cm	-180	rhizolith	-7.2	-7.4
22ESGR-whitestripe-160to180cm	-170	white matrix in bulk soil	-6.6	-7.7
22ESGR-bulk-160to180cm	-170	homogenized bulk soil	-2.7	-8.2
22ESGR-bulk-120to140cm	-130	homogenized bulk soil	0.2	-6.2
22ESGR-whitestripe-80to100cm	-90	white matrix in bulk soil	-6.0	-7.7
22ESGR-bulk-80to100cm	-90	homogenized bulk soil	-2.3	-7.0
22ESGR-whitestripe-70to80cm	-75	white matrix in bulk soil	-3.6	-6.8
22ESGR-sand-rhizo-290cm	-290	rhizolith	-6.1	-6.4
22ESGR-sand-rhizo-270cm	-270	rhizolith	-7.9	-7.4
22ESGR-sand-bulk-300cm	-300	bulk sediment	-1.2	-6.2
22ESGR-lowergravel-325to375cm	-350	bulk sediment	-0.2	-5.4
20EGSR-100-105-lst-clast	-100	limestone clast	-0.4	-6.9
20ESGR-70-75-lst-clast	-70	limestone clast	2.5	-7.7

[a] $\delta^{13}C$ and $\delta^{18}O$ data are generated via CO_2 on a Kiel Device. Typical precision is ± 0.1.

Table 3: Clumped isotope (Δ_{47}) and calculated $\delta^{18}O_{rsw}$ values for select carbonates from the Reserve

Sample ID	num Δ_{47} analyses	Δ_{47} ICDES-90 ‰	Δ_{47} ERR [a]	TΔ_{47} °C	TΔ_{47} ERR	$\delta^{18}O_{rsw}$ ‰ SMOW	$\delta^{18}O_{rsw}$ ERR
20EGSR-50	5	0.593	0.007	25	2	-4.8	0.5
20EGSR-slope-70-75	4	0.572	0.007	33	3	-3.5	0.5
20EGSR-slope-120	4	0.604	0.007	22	3	-6.3	0.5
22ESGR-rhizolith-180cm	3	0.622	0.008	16	3	-6.9	0.5
20EGSR-100-105-lst-clast	2	0.486	0.010	70	5	3.4	0.8
20ESGR-70-75-lst-clast	3	0.456	0.008	87	5	5.1	0.7

[a] Δ_{47} ERR is calculated as the larger of 1 SD of sample measurements or 0.014 (the long term SD of in-house standard 102GCAZ01) divided by the square root of the number of measurements

Table 4: Summary of Meteoric and Soil Water Isotope ($\delta^{18}O$, $\delta^{2}H$) Data

Water Type	Precipitation	River	Marsh	Soil
Slope	7.8	5.5	5.4	7.5
Intercept	11.8	-9.6	-8.2	3.5
r^2	0.98	0.91	0.95	0.90
observations	160	167	12	29
mean $\delta^{18}O$	-9.5	-7.3	-4.6	-6.6

Figure 1

Click here to access/download;Figure;Figure1.pdf

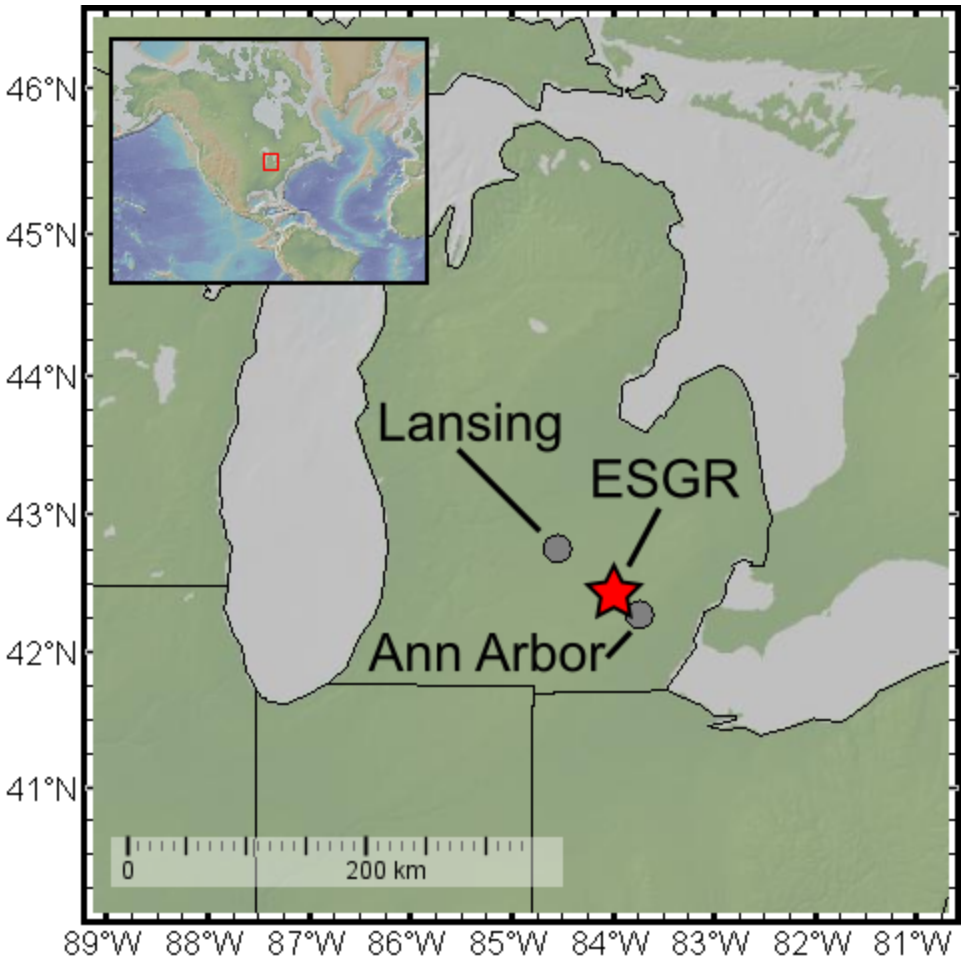

Figure 2

Click here to access/download;Figure;Figure2.pdf

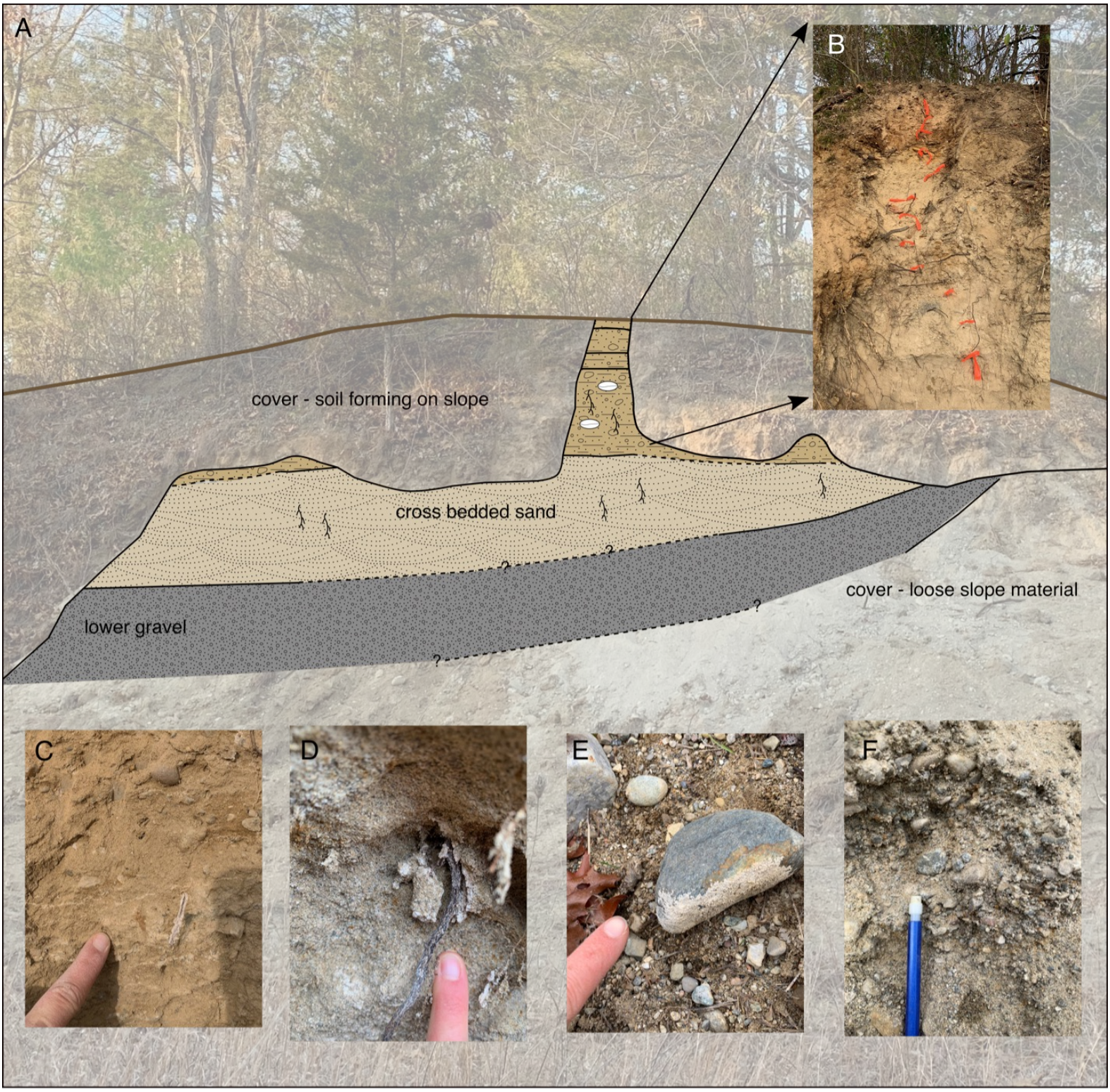

Figure 3

A) Stratigraphy and pedogenic features

B) Stable isotope values of soil carbonate

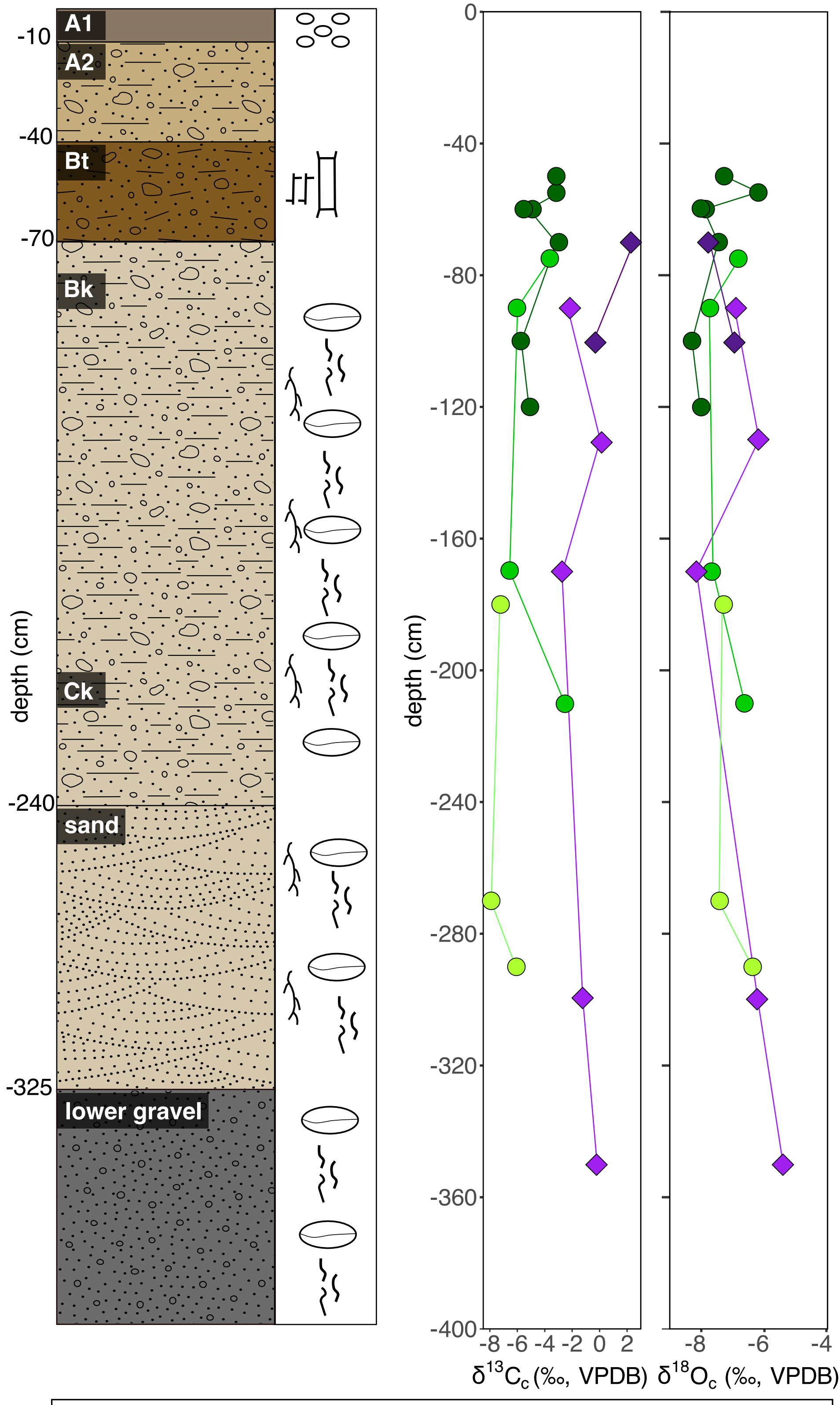

Figure 4

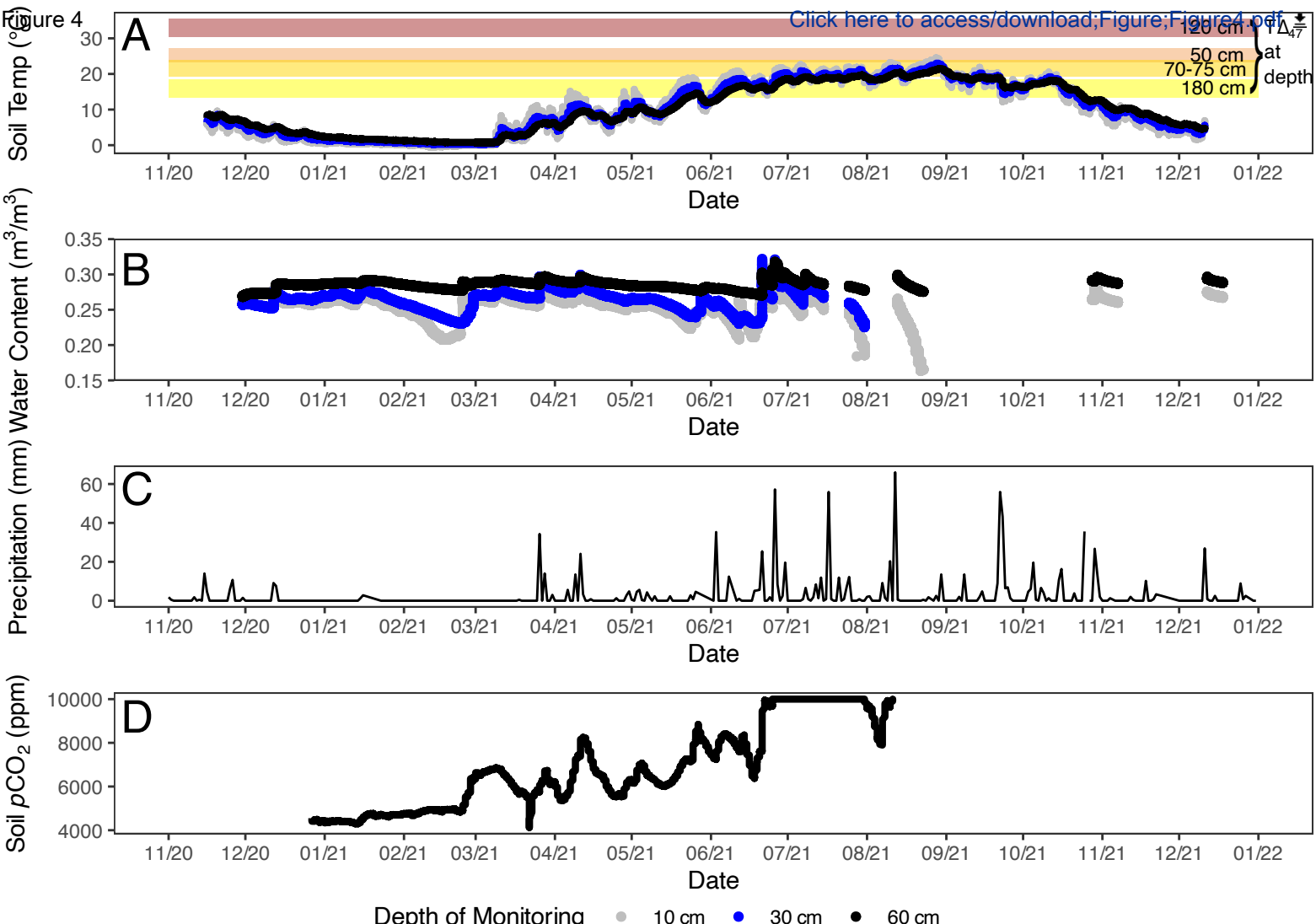

Figure 5

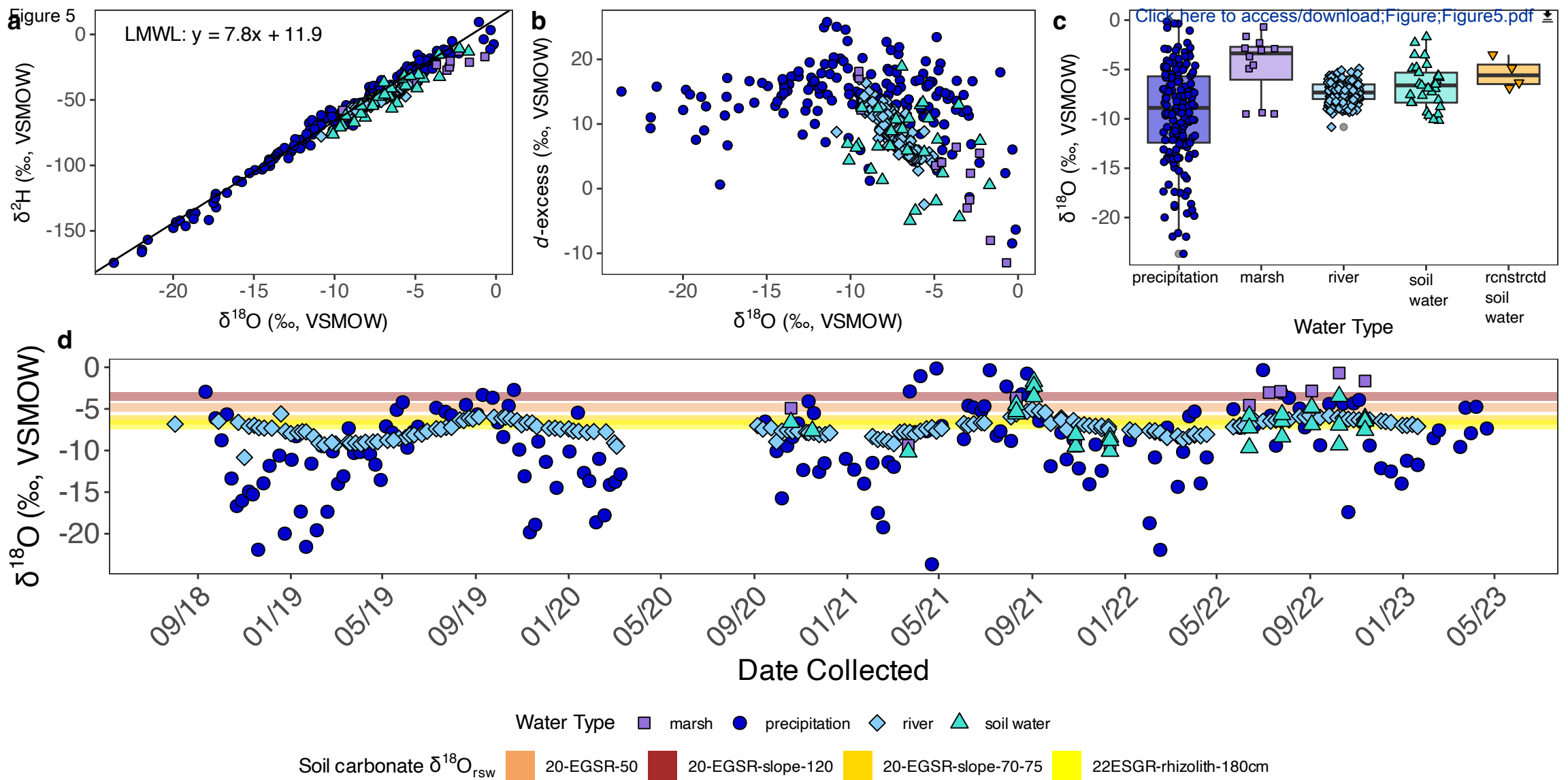
a
LMWL: y = 7.8x + 11.9
δ2H (‰, VSMOW)
δ18O (‰, VSMOW)
b
d-excess (‰, VSMOW)
δ18O (‰, VSMOW)
c
δ18O (‰, VSMOW)
precipitation
marsh
river
soil water
rcnstrctd soil water
Water Type
d
δ18O (‰, VSMOW)
09/18
01/19
05/19
09/19
01/20
05/20
09/20
01/21
05/21
09/21
01/22
05/22
09/22
01/23
05/23
Date Collected
Water Type
marsh
precipitation
river
soil water
Soil carbonate δ18Orsw
20-EGSR-50
20-EGSR-slope-120
20-EGSR-slope-70-75
22ESGR-rhizolith-180cm

Figure 6

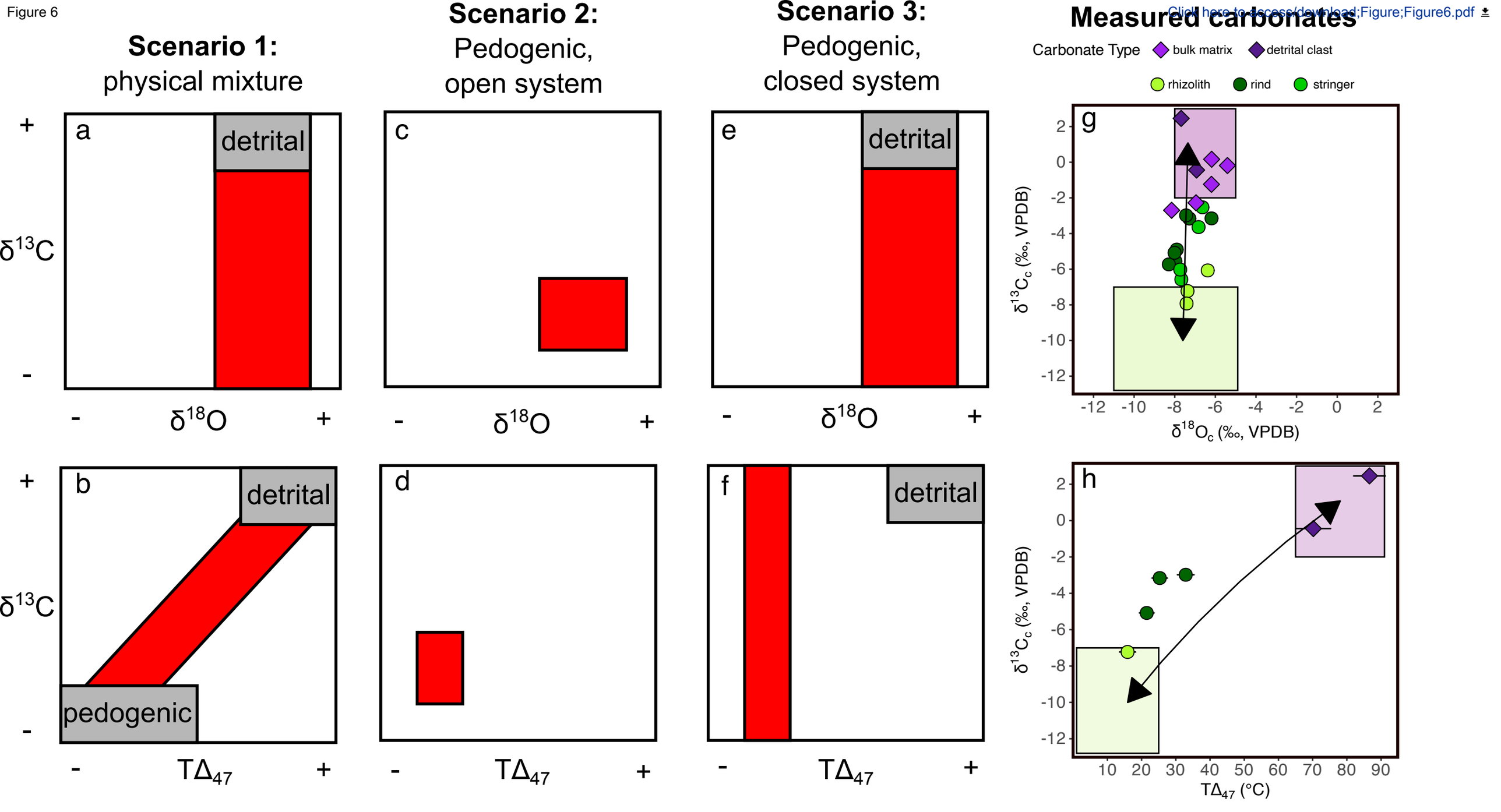

Figure 7

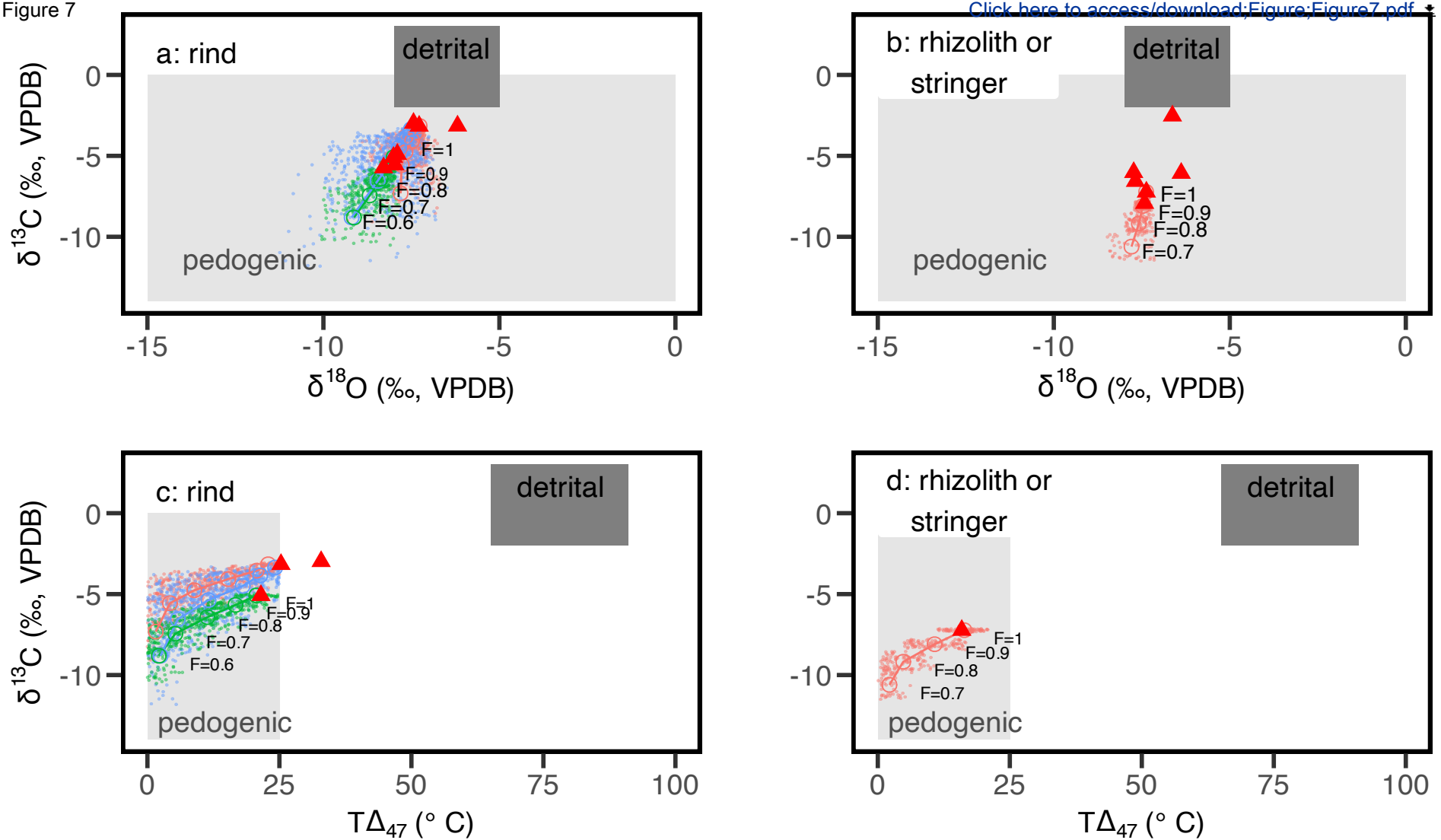

Figure 8